Acoustic Estimates of Distribution and Biomass of Different Acoustic Scattering Types Between the New England Shelf Break and Slope Waters

Thesis by,
Alexander McLaren

In Partial Fulfilment of the Requirements
For the Degree of
Master of Science

King Abdullah University of Science and Technology, Thuwal
Kingdom of Saudi Arabia

Approval date:

November 2011

EXAMINATION COMMITTEE APPLICATION FORM

The thesis of A. McLaren is approved by the examination committee:

Committee Chairperson: Prof. Stein Kaartvedt, Professor at King Abdullah University of Science and Technology.

Committee Co-Chair: Dr. Gareth Lawson, Scientist at Woods Hole Oceanographic Institution

Committee Member: Dr. Thor Klevjer, Scientist at King Abdullah University of Science and Technology.

ABSTRACT

Acoustic Estimates of Distribution and Biomass for Different Scattering Types Between the New England Continental Shelf Break and Slope Waters

Alexander McLaren

Due to their great ecological significance, mesopelagic fishes are attracting a wider audience on account of the large biomass they represent. Data from the National Marine Fisheries Service (NMFS) provided the opportunity to explore an unknown region of the North-West Atlantic, adjacent to one of the most productive fisheries in the world. Acoustic data collected during the cruise required the identification of acoustically distinct scattering types to make inferences on the migrations, distributions and biomass of mesopelagic scattering layers. Six scattering types were identified by the proposed method in our data and traces their migrations and distributions in the top 200m of the water column. This method was able to detect and trace the movements of three scattering types to 1000m depth, two of which can be further subdivided. This process of identification enabled the development of three physically-derived target-strength models adapted to traceable acoustic scattering types for the analysis of biomass and length distribution to 1000m depth. The abundance and distribution of acoustic targets varied closely in relation to varying physical environments associated with a warm core ring in the New England continental Shelf break region. The continental shelf break produces biomass density estimates that are twice as high as the warm core ring and the surrounding continental slope waters are an order of magnitude lower than either estimate. Biomass associated with distinct layers is assessed and any benefits brought about by upwelling at the edge of the warm core ring are shown not to result in higher abundance of deepwater species. Finally, asymmetric diurnal migrations in shelf break waters contrasts markedly with the symmetry of migrating layers within the warm ring, both in structure and density estimates, supporting a theory of predatorial and nutritional constraints to migrating pelagic species.

ACKNOWLEDGEMENTS

I would like thank Stein Kaartvedt for doing so much in aiding and abetting in the deviation of my would-be prosperous future in plundering the Saudi desert for oil, and for generously bringing me on the most exciting cruises in the Red Sea and Norway. I would also like to thank Stein along with Jim Luyten, Xabier Irigoyen, Micheal Berumen, Uli Stingl and Chris Voolstra for being passionate about the world they are exploring, the stories they tell and for their active inclusion of the students in the fascinating research they are bringing to the surface. This thesis was supported from two ends of the world by both Stein in Thuwal and Gareth Lawson at Wood's Hole, so I hope the pteropods are calcifying quickly. I benefited enormously from the advice and guidance of Thor Klevjer and Anders Røstad. I must thank G.Lawson, T.Stanton, D.Chu, and L.McGarry for the code that formed the basis of my acoustic analyses. I would like to thank Chuck Greene, his stellar team at the FHL Bio-acoustic course for an incredible introduction to the field amidst summersaulting killer whales. KAUST, for me, has been what it set out to achieve: a voyage of discovery.

I would like to thank the many friends I have met at KAUST, for un-regrettable relationships sprouted by coming to Saudi Arabia; I have enjoyed a front row seat suffering the ill-consequences of their brilliant ideas; they have confirmed to me that the true value in a university is created over the lunch table. If the academic experience of coming to KAUST wasn't enough, then it was worth coming just for the company.

Finally, I must thank my friends and loved ones for great support and patience through tough decisions over the last two years. Peering into the twilight zone has been a life-long dream as well as a luxury, and I hope to be able to unlock more stories waiting to be told from beneath the waves ...

"This is weird stuff!"

Stein as he looks on in bemusement at an indescribable echogram,
Red Sea Expedition, November, 2011.

TABLE OF CONTENTS

TABLE OF FIGURES

INTRODUCTION

The deep sea provides vital ecosystem functions including nutrient recycling, carbon sequestration and regulation of ocean chemistry and its largest component of biomass is likely to have an important role to play in them (Kelly, et. al. 2010) & (Pakhamov et. al., 1996). Mesopelagic fishes constitute a large fraction of the world's fish biomass. Global estimates for the largest representative population of mesopelagic fishes, the family Myctophidae - characterized by 250 species in 33 genera, ranges from $550 \bullet 10^6$ metric tonnes (Catul et. al., 2011) of a total mesopelagic fish biomass estimate of 1 billion metric tonnes (Gjosaeter & Kawaguchi, 1980). Such species inhabit the water column between 200 and 2000m and tend to be relatively small with a typical maximum size of 70-80mm; the majority are below 15mm (FAO, 1997). The family Myctophidae is one of the most common and abundant of the deep sea fishes accounting for approximately 20% of the oceanic ichthyofauna (McGinnis, 1982). Small pelagic fishes, and in particular mesopelagic fishes, play an important role in open oceanic energy dynamics as a link between trophic groups of primary consumers such as zooplankton and the higher levels of commercially targeted fishes like tuna as well as sharks and cetaceans (Catul et. al., 2011).

Mesopelagic fishes are a dominant component of the deep acoustic scattering layer. Some, though not all, perform extensive diel vertical migration (DVM) between the epipelagic and mesopelagic regions, foraging in upper waters at night and hiding in deep, darker waters during the day (Catul et. al., 2011).

Current interest in mesopelagic fishes is due to the state of full- or over-exploitation of most of the world's fisheries. There is an urgent need to investigate alternate resources and mesopelagic fishes represent one example of such alternative. Not only a populace component of the mesopelagic fish biomass (65%) (Hulley, 2011), members of the family

Myctophidae have come to occupy an important spot in percentage of total biomass trawled at some fishery sites, including landings and throw-backs; (Hulley, 2011) estimates this value at 10% of total pelagic trawls. One species *Benthesoma pterotum* is known to occur from the gulf of Oman to 25°S off the Mozambique coast. Estimates of biomass at $18 \bullet 10^6$ metric tonnes make this the largest single species fish biomass in the world (Hulley, 2011).

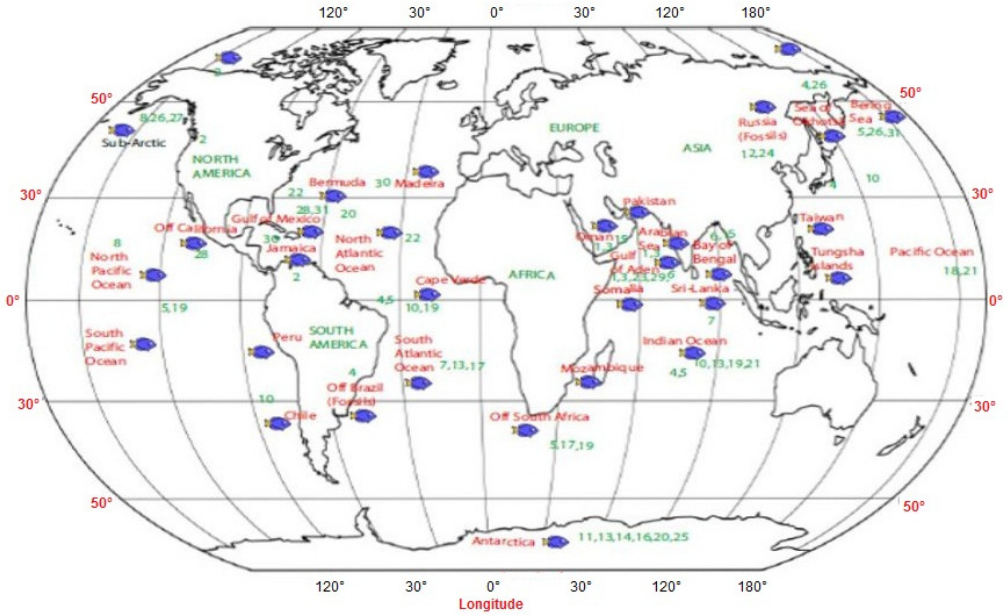

Figure 1: World map of possible global distribution of the family Myctophidae (Catul et. al., 2011).

The distribution of mesopelagic fishes encompasses all oceans except the Arctic, Figure 1. A review on pelagic fishes by (Catul et. al., 2011) gives a graphic representation of the possible global distributions of *some* myctophid species. A two-year data base started in the 1990s by the Northwest Atlantic Fisheries Organization to sample mesopelagic zooplankton and fish in the NECS region indicates that the prevalent species were Benthosema glaciale, Lobianchia dofleini, Ceratoscopelus maderensis and Hvdophum hvoomii (Stern & Serchuk, 1992). Backus' 1967 Alvin expedition discovered large agglomerations of Cetoscopelus madrensis 10 to 100 meters in diameter near the site of this study (39°48'N, 70°33'W)(Backus et. al., 1968). Furthermore, data on acoustic estimations of biomass can be used to map potential prey fields, and is one of the intended uses of such data.

Differences have been observed in the latitudinal distribution of mesopelagic fish species in the North Atlantic Ocean which can be related to the oceanic circulation. The Gulf Stream system gives rise to a discontinuity in the position of the north wall of the Gulf Stream. This front represents a sharp boundary between subpolar and subtropical waters along the northern edge of the Gulf Stream. The discontinuity of the north wall of the Gulf Stream results in a broad zonal range extension of midwater fishes to the North and North-East. An analysis of the fishes captured during the International Overflow '73 Expedition of ICES confirms the well-known earlier observations of an unhampered northward drift of many temperate and subtropical species up to the secondary Polar Fronts (Krefft, 1976).

There are several studies attempting to assemble ecological and environmental data for the analysis of the distribution of the family Myctophidae in the East Antarctic (Moteki, Koubbi, Pruvost, Tavernier, & Hulley, 2011), the Arabian Sea (Kinzer et. al., 1993), the Gulf of Mexico (Ross, Quattrini, Roa-Varon, & McClain, 2010) as well as in the subarctic Pacific gyres (Bemaish et. al., 1999). Most studies in the NECS region are concentrated on the shelf between 41°N and 43°N, nearer the more productive fisheries. Studies in or near our area often focus on other types of fauna such as (Boyd, Wiebe, Backus, & Craddock, 1986) on micro-nekton, (Lavery et. al., 2007) on zooplankton and (Wiebe, et. al., 1996) on zooplankton.

The major current systems of the North-West Atlantic are the Labrador Current, the Gulf Stream, as they interact with Shelf and Slope Water currents (Chapman & Beardsley, 1989). Both deep-water influxes and frontal interactions (such as the north wall of the Gulf Stream) mix shelf and slope waters. Frontal systems dominate throughout the North-West Atlantic shelf region, producing marked heterogeneity of biological and physical features, and thus producing identifiable bio-geographic regions between hydrographically distinct watermasses (Robinson & Brink, 2004). Movement of the shelf/slope front is dictated largely by warm core ring activity, evidence suggests a relation between the position of the front and larval abundance in the region (Bolz, 1978).

The shelf break, continental slope and deep sea region associated with the New England Continental Shelf Region (NECS, 37-43°N and 63-71°W) is a relatively unexplored region of the North-West Atlantic and is adjacent to one of the most productive fisheries in the world with an extensive history of exploitation: the Georges Banks Complex (Kelly et. al., 2010), (Mayo & Serchuk, 1987) & (Wiebe et. al., 1996). The deep sea, defined as depths below the shelf break ~200m, is the largest ecosystem on the planet, comprising 63% of the surface of the Earth (Kelly et. al., 2010). The vast majority of deep-sea regions are under-sampled and previous sampling efforts have been highly variable over both spatial and temporal scales.

A marine mammal survey cruise conducted by the U.S National Marine Fisheries Service (NMFS) in August 2009 provided the opportunity to explore this remote and rarely studied region. Acoustic data collected during the survey allowed a study down to 1000m depth to investigate the distribution, migration and acoustic estimates of biomass of the mesopelagic realm. That attention to the mesopelagic realm is firstly dictated by the bathymetry of the region and the range of the acquired data, but also motivated by recent findings that indicate a large biomass associated with the mesopelagic in the NECS region (Backus et. al., 1968) (Badcock & Merrett, 1975).

Previous work shows highly variable faunal composition on and off the shelf and reduced taxonomic diversity indicative of distinct faunal assemblages above seamounts, on the continental slope, the shelf edge, canyons and the continental rise (Kelly et. al., 2010). Although no data could be found for the NECS, fish stock assessments in other large fisheries are recording sharp drops in biomass landed, accounted for mostly by a drop in mesopelagic fish (Myctophid) landings (CCAMLR, 1993) or an increase in the proportion of catch attributed to mesopelagic fishes (Hulley, 2011). This is especially concerning for a organisms that are poorly studied in terms of biomass, distribution and life history. The productivity of the Georges Bank complex has supported an increase in active fishing vessels from 220 to 345 between 1994 and 2007, helping to propel Massachusetts to the leading position in the USA for value of landings for the last eight years (NEFMC, 2011).

The ship track covers regions along the shelf between 67° and 73° W and moves out over the continental slope through the unique ecosystem of a warm core ring, mapping the distribution of scatterers horizontally and vertically. In our analysis, data from (Badcock & Merrett, 1976) covering an area bounded by 29°37'-30°13'N and 22°55'-23°17'W in the Northeast Atlantic, will serve as comparison for length distributions and biomass associated with diel vertical migrating and non-migrating scattering layers. This phenomenon is known as Diel Vertical Migration and will be referred to as DVM throughout the text.

The use of acoustic methods to estimate animal biomass density (g/m^3) requires information of the acoustic size, backscattering cross section and a weight to length function for individual organisms associated with the observed acoustic backscatter. The total backscatter recorded will be a function of the amount of acoustic energy reflected from the incident wave by the target (and dependent on the targets' acoustic backscattering cross-section). This problem is commonly synthesized into what remains and under-determined problem; where a greater number of size classes can potentially make up the recorded

acoustic backscatter recorded. The more information that can be provided the better our ability to resolve the correct size distribution of targets. More information is obtained by observing the same scene simultaneously by a range of frequencies using multi-frequency or broadband techniques. The variation that individual targets present across a frequency range is known as the frequency response and will vary according to physical properties of the target such as whether or not it has a gas inclusion, and can be used to identify the target in question (McLennan & Simmons, 1992). The frequency response of the target will further vary based on the target's acoustic properties, general size and shape. This paper will make use of this method to search for consistently occurring and distinguishable frequency responses in order to separate the acoustic backscatter in the water column according to acoustic scattering types, follow their migrations and distributions and in order make inferences on their size and biomass density.

The purpose of this study is to discuss scatterer distributions and migrations on and off the shelf and their variation with environmental and biological data in the NECS region. This is done by identifying acoustically distinct taxa to support the development of acoustic models specific to the frequency responses observed in the data. Finally, I define and suggest explanations for the observed differences in abundance, distribution and changing structure in migration patterns across the different environments intercepted during the cruise.

MATERIALS AND METHODS

Data Collection

The project was conducted as part of the 6-16th August 2009 shakedown cruise in preparation for the National Marine Fisheries Services' Marine Mammal Survey, conducted in July 2011. Data from this NMFS cruise was provided by Mike Jech with the support of Gareth Lawson from Woods Hole Oceanographic Institution (WHOI) and Stein Kaartvedt at King Abdullah University of Science and Technology (KAUST) through the KAUST/WHOI partnership. Acoustic data was collected aboard the NOAA ship Henry Bigelow at 18, 38, 120 and 200 kHz on a scientific echosounder, Simrad EK60. The ship is also fitted with a variety of navigation, communication and other acoustic instrumentation including ME-70 multi-beam sonar, ES-60 echosounder, RD Instruments acoustic Doppler current profiler and a Furuno FE-700 navigational echosounder(NOAA, 2011). From the data acquired, it is clear that at least two or more of these instruments interfered with the EK60 data collection leaving intense sound spikes in our data set. Also, due to the objective of the cruise of quantifying marine mammal abundance using passive acoustic and visual counts, data was not collected for long intervals during daylight hours whilst visual surveys for marine megafauna were being conducted. Nevertheless, significant data across the shelf region and over the continental slope allows for a comparison of data within and across these areas, although reducing the data acquired over the 11 day cruise to two diel vertical migrations over the NECS region and another two over the continental slope.

Conductivity-Temperature-Depth (CTD) data was acquired using the Seabird Electronics SCE model 19+ profiling CTD (s/n 4684 for bongo and water casts and s/n 4477 used for Video Plankton Recorder – VPR - tows)(NOAA, NOAA Fisheries Service, Marine Mammal Survey, 6-16th August, 2009, HB 09-03., 2009).

Sampling Bias

Graphs illustrating the sampling bias inherent in the data are presented below as the frequency of data recorded at various times of day and location defined by distance from the NECS shelf break region. Less than seven percent of registered pings, in fact, occurs between 0500hrs and 1400hrs over the entire cruise. For the reason illustrated in the sampling bias graphs, the more relevant information in the data is likely to come from the range and variation of ($s_{A|d}$) with each parameter rather than the density of data. High ($s_{A|d}$) is a result of well distributed intense backscattering within the water column, and increased range of ($s_{A|d}$) above a threshold of 50dB is indicative of a dense and dominant DVM. The histograms are produced for data which omits sections that do not have information at all frequencies or which do not have information to the full depth of the water column. Tight looping in the vessel track data was also deliberately removed from the data set to reduce the potential for oversampling a given region.

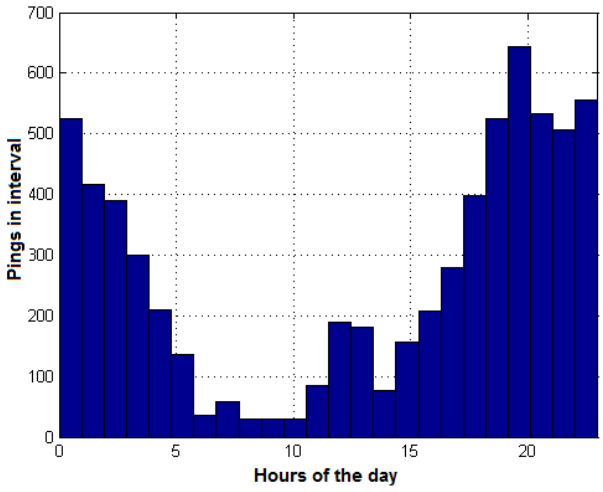

Figure 2: Frequency of data collected at hourly intervals throughout the day. Bias is a result of reduced monitoring during the day to allow for passive acoustic and visual surveying of marine mega fauna.

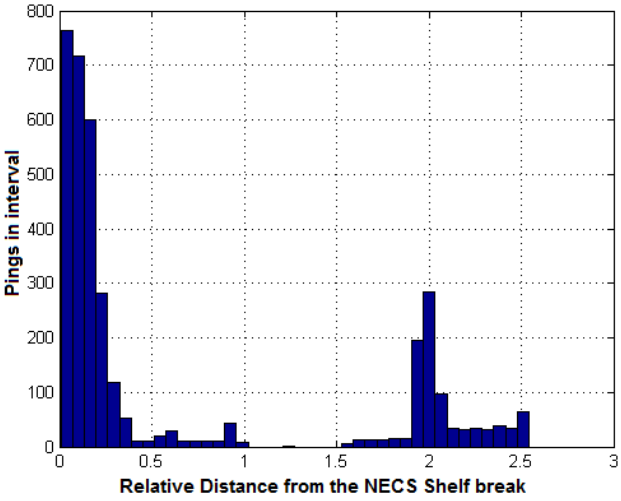

Figure 3: Spatial distribution of acoustic sampling relative to the shelf break. Survey sampling bias; most samples are taken along the GBK shelf or out over the continental slope (4000m depth), hence analysis is limited to a qualitative near and off-shelf comparison.

Acoustic measurements

Measurements of volume backscattering strength (S_v – units: decibels relative to 1 m^2/m^3), and target strength (TS - units of decibels in m^2), were made continuously through the trip where and when visual surveys for marine megafauna were not underway:

$$S_v = 10\log_{10}(s_v) \quad (1)$$

$$TS = 10\log_{10}(\sigma_{bs}) \quad (2)$$

Volume backscatter is defined as the ratio, of backscattered intensity produced by unit volume at one meter from the volume, to the intensity of the incident wave. Target strength (TS) is defined, by equation 2, as 10 times the logarithm of the reflected intensity at one metre from the fish, divided by the intensity which strikes the fish (FAO, FAO Coprorate Document Repository, 2011). In this way, TS does not account for volume and instead returns information relevant to all insonified organisms, making this measurement key to density estimates.

In Eq.1, s_v is the volume backscattering coefficient, a measure of the intensity of emitted sound that is reflected back to the source per cubic meter; and in Eq.2, σ_{bs} is the differential backscattering cross section. Measurements were made by a hull-mounted (~6m depth) EK60 split-beam echosounder at 18, 38, 120 and 200 kHz to maximum ranges of ~1000, ~1000, ~200 and ~200m respectively. Some error exists in that the echosounder is situated in the tip of a retractable keel below the NOAA ship H.Bigelow and so the depth of the actual echosounder could vary between 2 and 6m (personal communication with Erin Lebreque). Acoustic data was collected at 10kHz regular continuous width pulse at a ping rate of 0.3 pings/s, and the range of backscattered energy attributed to biological targets spanned -85 to -40 dB. The vertical resolution of the data after processing was 1.5m at 18 and 38kHz and 1m at 120 and 200kHz; echo integration was performed over intervals corresponding to a horizontal resolution of ca. 100m depending on the ships speed.

The transducers (manufacturer Simrad, Kongsberg Maritime, Norway) were calibrated *in situ* prior to the survey with standard targets (tungsten carbide, 6% cobalt spheres of diameter 38 and 21mm) during August 2009. It was not feasible to assess any depth-dependence of the system during the calibration procedures. While over the NECS region it was observed that the sea-floor backscatter strength varied by less than 0.5 dB, depth-related changes in the system are then likely to be smaller than 1dB and are unlikely to affect any biological conjectures made from the data set.

Acoustic Analyses

Procedures for dealing with noise

For the task of dealing with the noise spikes associated with interference from other acoustic instruments, an attempt was made in the first instance to threshold, but this entailed the deletion of some biological backscattering. In the second instance an attempt to filter or distribute the noise spike using a 3-by-3 and 4-by-4 convolution matrix, but this also led to the loss or reduction in quality of biological data of interest. Finally a spike-filter developed by Tim Ryan (Echoview, 2009) from a method in the paper (Anderson, Brierley, & and Armstrong, 2005) was employed to remove noise spikes from the data set. This method first aligns all echograms and then they are shifted n and n*2 pings. A check using the formula operator function in echoview is made to look for characteristic rises or falls in the volume backscatter by a threshold amount that last n pings. In the function below, V_1 is the original ehogramme, V_2 is shifted n pings across and V_3 is shifted 2*n pings across, X_{dB} , Y_{dB} , and T_{dB} characterize the expected variation introduced by noise spikes for relative increase and base threshold.

$$f(\mathbf{p},s) = not(V_1 - V_2 > X_{dB} \; and \; V_1 - V_3 > Y_{dB} \; and \; V_1 > T_{dB}) \qquad (3)$$

In our case, n=1, and X_{dB} = 10, Y_{dB} =10, and T_{dB} =-80 in units of decibels.

Noise within the data set also appeared in the form of a reduced signal to noise ratio with an increase in depth due to the time-varied gain, which amplifies recorded acoustic signals with the time interval between each ping's emission in order to allow data to be comparable across depths. The consequence of this, along with the greater loss of acoustic energy at higher frequencies due to absorption and spreading, was the necessity to look at our data in layers (McLennan & Simmons, 1992). For the deeper data, beyond 200m, where the 120 and 200kHz echosounders were not available analysis relied solely on 18 kHz and 38 kHz data for

acoustic scatterer classification. Above that depth use of all four frequencies was possible. In order to deal with noise, the (De Robertis & Higginbottom, 2007) method was used, in which all signals below a signal-to noise ratio are deleted. The noise is defined by the appropriate artificially generated time-varied gain function, to reproduce the observed noise in the data. It is then subtracted from the data to develop a signal-to-noise ratio. It was nevertheless necessary to cut off the extent of our echograms since the method has more limited effect with depth.

Selected cruise tracks for acoustic analysis

The acoustic data chosen for analysis is a trade-off between segments designed to give a good representation of variations between the continental shelf break and slope of the NECS system and the potential for acoustic analysis and interpretation. The criteria were the presence of 3 or more frequencies in sequence for the upper 200m to cover shelf break and adjacent deep water at ca. 4000m depth, in and out of the warm core ring for transitions across day and night. Not all of these objectives could be met, but data in each category is available and portions of, if not the full cycle of diel vertical migrations are available on the shelf and in the warm core ring.

Data from the shelf slope was allocated to four regions: Region I [N39°51’ W71°64’ to N40°95’ W71°64’] night transitioning into day, Region II centred over [N39°05’ W72°21’] day transitioning into night, Region III [N38°45’ W73°81’ to N38°70’ W72°24’] both day and night transects. For analysis off the shelf slope two regions were in ca. 3000m of water and the third in ca. 4000m of water. The Regions are: Region V [N39°21’ W68°92’ to N39°63’ W68°89’], Region IV centred over [N37°51’ W69°05’]. The total data analyzed was for four overnight periods including one full day of data over the warm core ring.

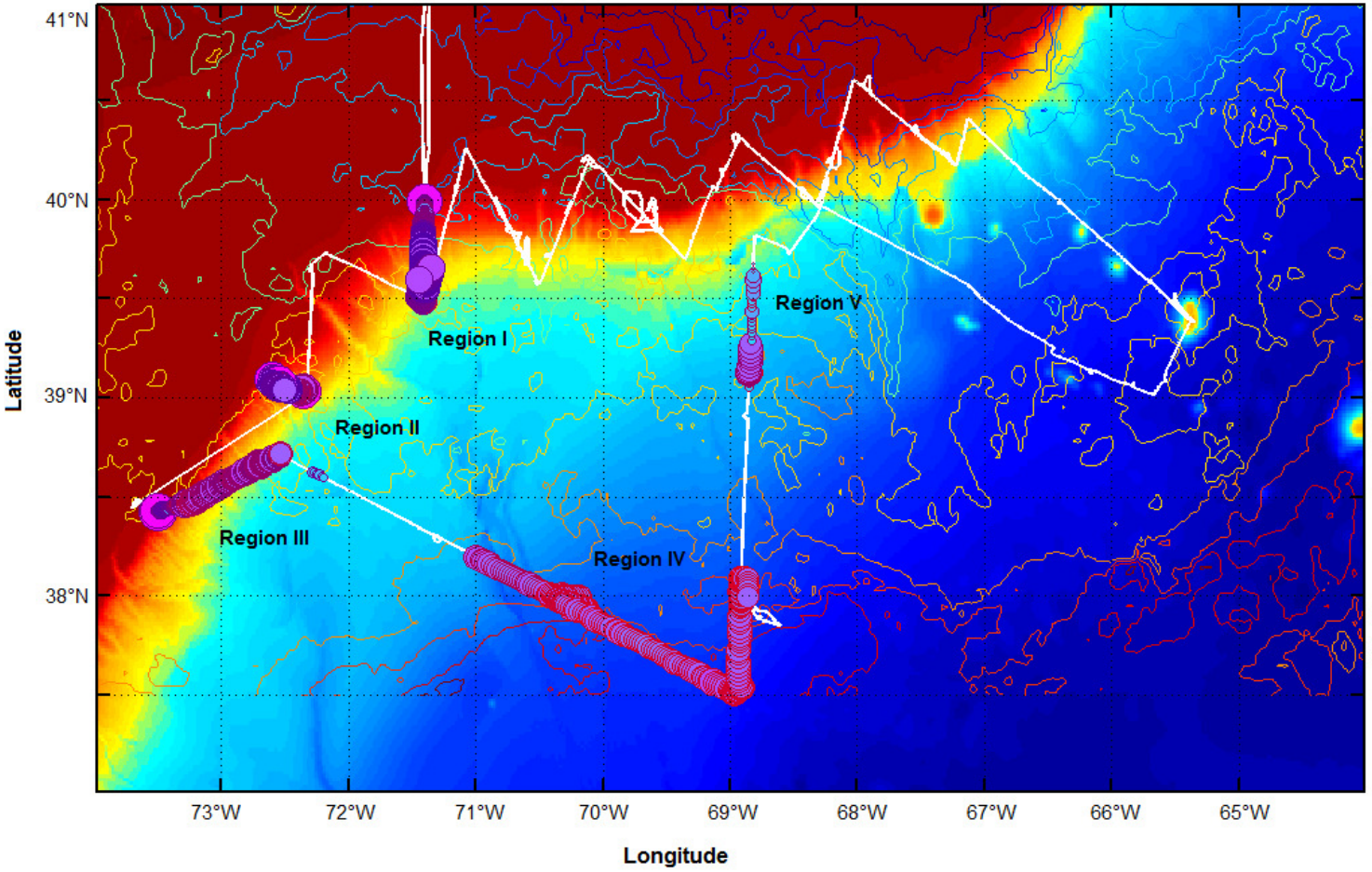

Figure 4: NOAA Ship H.Bigelow track during the 6-16th August 2009 Shakedown cruise for the NFMS Marine Mammal Survey in 2011. The surface temperature contours, ranging from 10°C to 25°C, is superimposed on bathymetric gradient ranging from 100m depth to 4000m depth (NOAA, Coastwatch West Coast Regional Node, 2011). Full track is shown in white and total volume backscatter is indicated by the relative size of the circles ranging between -70 and -40 dB re m-1.

Identifying acoustically distinct taxa by frequency response

Various methods for the classification of acoustic data into types of scatterers exist. All capitalize on the fact that the acoustic energy returned from an organism across different frequencies in an insonified volume will depend on its anatomy, material properties (hence depth, diet and life history) and size. From these parameters it is possible to build complex or as simple a frequency response model for the interpretation of the backscattered acoustic energy into ecologically relevant information of length distributions and biomass. Such acoustic methods are complicated to a great degree by the intervention of so many parameters, such as size, shape, orientation, acoustic properties and the composition of the layers they are found in. This means that the backscatter will be indirectly related to the physiology and life history of organisms, their depth, and diet. Nevertheless, the participation of such parameters in the backscattered energy recorded mean that these methods have the potential to resolve each of these factors. Myctophidae, with an acoustically varied life history among species, will sometimes bear swim bladders to facilitate buoyancy during juvenile stages, which become filled with lipids or degenerate during maturation (Moser and Watson 2006). Hence weaker backscattering, in this case, would be expected from the larger adults of the population and this complicates the method of pairing target strength values and distributions to length estimates and distributions.

In all cases a sequence of condition filters is built to pass data from the original echogrammes through to a final masked image that shows only those regions of backscattered energy that match the characteristic frequency response of a distinct scattering type (*cf.* Figure 13). In this way the aim is to disassociate “acousticly distinct” taxa, i.e sorted not according to phylo-genetic criteria but simply according to acoustic criteria.

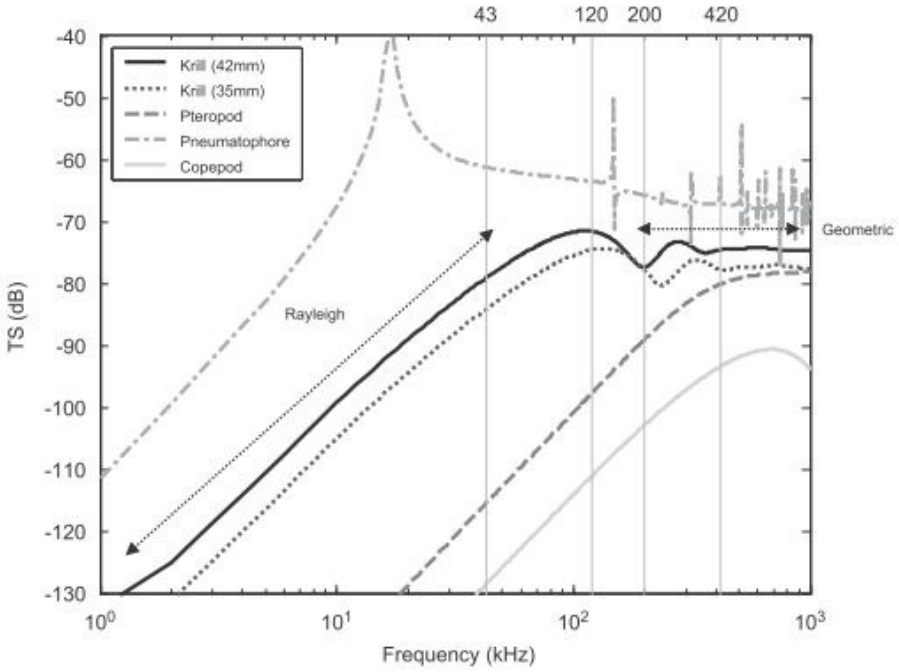

Figure 5: Target strength in relation to acoustic frequency. Predictions made using physics-based models for 35-42mm long krill, 1mm pteropod, 1.5mm diameter siphonophore and a 2mm copepod. Illustration of size and shape dependance of acoustic backscatter (Lavery et. al., 2007).

In this study relative frequency response between each pair of frequencies is combined in sequence, such that each additional frequency pair adds another level of determination attributing scattering to one or another scattering type. The method proposed here attempts to look for consistent and widespread frequency responses contained in the data set by reference to areas that stand out in the raw echograms (Raw Sv at 18 kHz for example) or in the subtracted echograms (ΔdB between 38 kHz and 18 kHz). The results are resolved into scattering types that satisfy a set of conditional rules to allocate a scattering identity. An example of such frequency responses and the variation that leads to the setting of conditions is given below.

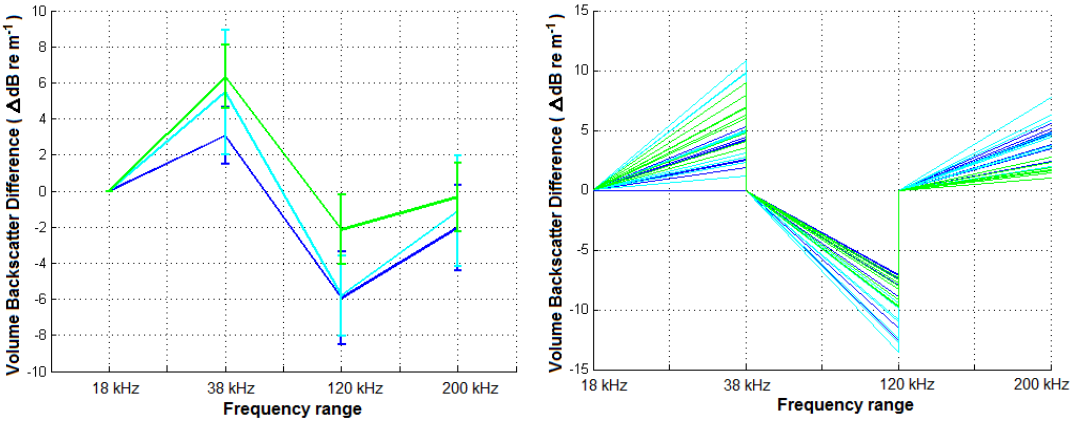

Figure 6: Example of how sequential conditions for classification within scattering types were determined. The dB differences between frequencies illustrated on the right are used as a sequence of filters to classify the frequency response illustrated left. All samples are taken from the warm water over the continental slope at daytime in the top 80m.

Different frequency responses are defined as a separate scattering identity depending on their potential resolvability as well as whether or not they come from areas of the echogram that can justify them as being distinct. Frequency responses of any kind are admitted at this stage and will not be disqualified until their interpretation based on well-documented expectations for the scattering of organs and organisms with different acoustic properties. For example, gas bubbles are expected to resonate acoustically when intercepted by acoustic energy at low frequencies and hence, higher backscatter is expected near the resonant frequency in the lower ranges. The frequency response therefore allows resolution between regions that scatter more strongly at 18kHz, and are interpreted to represent a region populated by organisms containing a swimbladder larger than 1.1mm diameter or a fluid-like scatterer larger than a 45mm long bent cylinder[1]. The conditions under which the data were collected limit available signals to those exceeding the threshold of -85dB.

Acoustic classification methods, although based around physical models and principles, often draw heavily on the groundtruthing data obtained via fish hauls or plankton nets to focus the options available for potential frequency response models. In our case, a more heuristic

[1] L/W = 2*8.2, g=1.03, h=1.03 is accepted for *Meganyctiphanes norvegica* (Gareth Lawson personal communication); for this result we use L/W=4.27, g=1.035, h=1.055 (Yasuma, 2006) for a Myctophid.

approach similar to that of (Jech & Micheals, 2006) will be applied. The implications of this are that the observed variation within the data across frequencies that *does* exist will be used to categorize distinct loci on the echogram. The author makes no attempt to identify scattering organisms until the discussion section where identification and comparison with scattering models such as (Lawson et. al., 2006) and (Gauthier & Horne, 2004), is necessary for estimates of length distributions and biomass. Due to the loss of information at higher frequencies with depth, the lower portion of the data, below 200m, will be interpreted separately and cannot make use of the above method due to the impossibility of isolating similar frequency responses across four frequencies, and identifying them with an appropriate model. In this case, it is possible make use of any resolvability available through variation in frequency responses between 18 and 38kHz. Any resulting classification method will, undoubtedly, be less accurate than the first, to which it will be compared in order to assign a measure of confidence in the resulting classification at depth.

Size class and length distributions

Length distributions are obtained for scattering layers by capitalizing on the fact that backscatter from organisms is dependent on size, frequency as well as on the organism's anatomy. By using the backscattering strength information at different frequencies of concurrent loci of the echograms a multi-frequency inversion using the linear least squares non-negative constraint can be used to estimate length distributions within aggregations. Lengths discussed in this report are acoustic lengths defined as the distance along the curve of the organism from the anterior tip of the rostrum to the posterior end of the uropods for a euphausiid-like scatterer. Since the focus in discussion will be shifted toward biomass and relative comparison of acoustic lengths, acoustic length is used as an approximation to the

standard length of the scatterer and an idea of order of magnitude for other organisms within this scattering type.

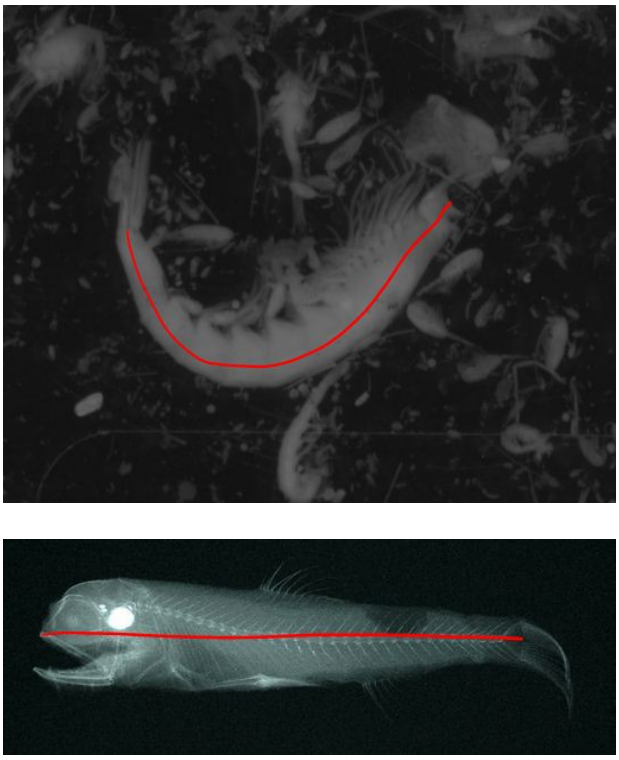

Figure 7: Illustration of the acoustic length of a Euphausiid (above) and Myctophid (Below). Krill sample taken from the July 16 Saanich Inlet cruise led by Charles Greene. Active acoustics, Mapping the diel distribution and migration of Euphausiids. [48°38'22.44"N 123°30'07.98"W]. Sample is viewed within the Digitizer programme developed by Copeley, N. And Wiebe, P. H. Myctophid sample from (Yasuma et. al., 2010).

The code used adapted from code developed by van Holliday for the Tracor Acoustic Profiling System (TAPS) and edited by C.Bassett, R.Levine and A. McLaren at Friday Harbor Laboratories, July 2011. Eq. 4 is solved and optimized using a non-linear least squares algorithm discussed in (Lawson & Hanson, 1973). Eq. 4 must be optimized based on frequencies and size classes in the simulation where, $\sigma_{v,f}$ is the total volume backscatter at each frequency, σ(f,a) is the TS for an animal of a specific size, a, at a chosen frequency, *f*, and N is number of animals in the size class. Values for σ are calculated for each inversion based on the frequencies, sizes classes, length to diameter ratios, and g and h values.

$$\sigma_{v,f_1} \approx N_1 \cdot \sigma(f_1, a_1) + N_2 \cdot \sigma(f_1, a_2) + \cdots + N_m \cdot \sigma(f_1, a_m)$$

$$\sigma_{v,f_2} \approx N_1 \cdot \sigma(f_2, a_1) + N_2 \cdot \sigma(f_2, a_2) + \cdots + N_m \cdot \sigma(f_2, a_m)$$

...

$$\sigma_{v,f_n} \approx N_1 \cdot \sigma(f_n, a_1) + N_2 \cdot \sigma(f_n, a_2) + \cdots + N_m \cdot \sigma(f_n, a_m)$$

(4)

This method depends on a validated TS distribution over the frequencies employed in our study, and this model should be validated for local species. The organism modelled is simplified down to the form of a bent cylinder and a number of assumptions are made: firstly, time and depth are assumed not to affect the acoustic properties of organisms. To expand on this, the assumption is made that the relative speed of sound between the organism and the water column is constant and independent on level of feeding or starvation and pressure or temperature – all of which are varying together in migrating species. Finally, a random normal distribution is assumed for the orientation of organisms to build the physical model within a range identified for a particular species.

One method for abundance estimates is to take the identified volume backscatter divided by the target strength identified for individual organisms.

$$N = 10^{\left(S_v - \tilde{TS}\right)} \quad (5)$$

In Eq. 5, (S_v – units: decibels relative to 1 m^2/m^3) is the volume backscattering strength, and ($\tilde{TS}$ - units of decibels in m^2) is the mean target strength for the same area. Models used in this report were applied principally to two scattering types: scatterers bearing a swimbladder and fluid-like bent cylinders without a swimbladder. Length classes resulting from the inversion process are lumped into three categories of small (copepod-sized), medium

(Euphausiid or Fish larvae sized) and large (Myctophid-sized) bins, in order to give coarse resolution on the relative length distribution within samples and inform us on potential identities.

Fish without swimbladders

In the case of bladderless fish, the theoretical investigation of the acoustic characteristics entails special difficulties (Kalikhman & Yudanov, 2006). Fish have a complex configuration and internal structure and incident waves will insonify various parts of its body at different times and at different angles. The distorted wave-born approximation model for a bent cylinder of (Chu et. al., 1993) and (Stanton et. al., 1993) is used, but as it is parametrized in (Lawson et. al., 2004). The total volume backscatter for the distributions is calculated using a length to diameter ratio of 8, specific gravity of 1.035 and an internal speed of sound relative to water at standard temperature and pressure, h, value of 1.055 (Yasuma et. al., 2006).

Euphausiids

In the case of Euphausiid-like scatterers the distorted wave-born approximation model of (Chu et. al., 1993) and (Stanton et. al., 1993) is used, but as it is parametrized in (Lawson et. al., 2006). The total volume backscatter for the distributions are calculate using a length to diameter ratio of 16.4, specific gravity of 1.038 and an internal speed of sound relative to water at standard temperature and pressure, h, value of 1.041 (Lawson et. al., 2004). The models incorporate an assumption that targets are distributed randomly about a mean angle of incidence relative to horizontal of 0° with a standard deviation of 27° (Backus et. al., 1968).

For estimates of biomass for scattering types identified at depth, the acoustic properties of the attributed ID will be assumed and the inversion will operate in the same way as for

length distribution and biomass estimation for data in the top 200m, but using the information at 18 kHz and 38 kHz.

Fish with swimbladders

The model for fish with swimbladders was developed using a fluid-like bent cylinder scattering model combined with a scattering model for a penetrable gas-filled sphere with the parameters set for air at standard temperature and pressure (Turley, unknown) (Sullivan-Silva, 1st November1989). The fluid-filled sphere model provided by G. Lawson, WHOI was adapted for the penetrable gas-filled model and reduced everywhere by 8dB such that it would match values obtained from literature on the scattering observed in mesopelagic fish from international publications[2] whilst maintaining the frequency response for a gas inclusion. The same parameters as the bladderless fish bent cylinder model are used and the resulting frequency response is illustrated below.

[2] (Sawada, Uchikawa, Matsura, Sugisaki, Amakasu, & Abe, 2011), (Yasuma, Sawada, Takao, Miyashita, & Aoki, 2010), (Davidson, 2011), (Godo, Patel, & Pedersen, 2009), (Benoit-Bird, 2009), (Reeder, Jech, & Stanton, 2004), (Benoit-Bird & Au, 2006), (Bolz, 1978) & (Ha, 2008).

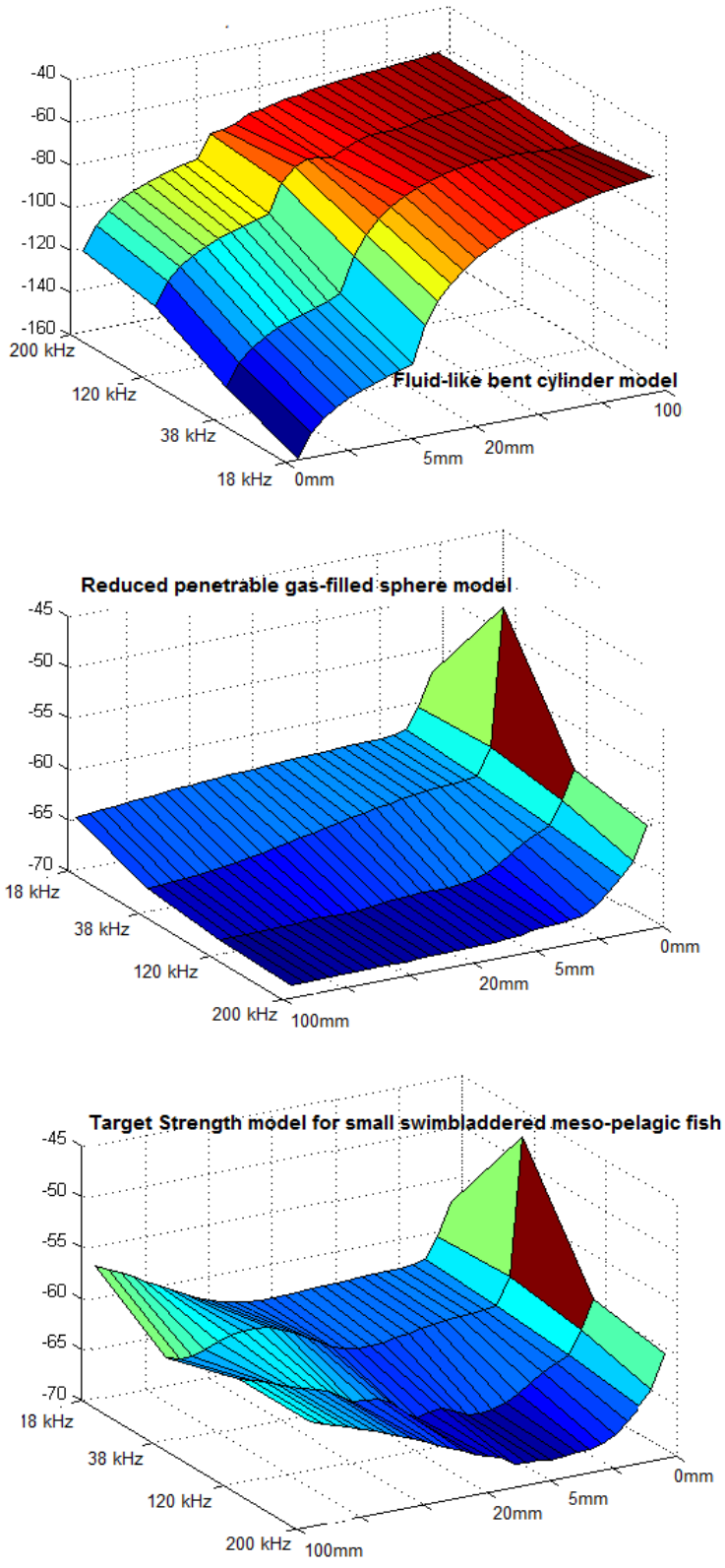

Figure 8: Development of the Target Strength model for small mesopelagic fish with swimbladders. Variation of TS is given with standard length of the fish and frequencies between 18 and 200 kHz. Penetrable gas-filled sphere model is reduced to allow rough agreement of the model with values observed in (Sawada, Uchikawa, Matsura, Sugisaki, Amakasu, & Abe, 2011), (Yasuma, Sawada, Takao, Miyashita, & Aoki, 2010), (Davidson, 2011), (Godo, Patel, & Pedersen, 2009), (Benoit-Bird, 2009), (Reeder, Jech, & Stanton, 2004), (Benoit-Bird & Au, 2006), (Bolz, 1978) & (Ha, 2008).

Biomass density estimates

Estimating biomass is one of the goals of this study. (Hewitt & Demer, 1993) shows that estimates of biomass are less sensitive to error associated with the assumed mean length than are estimates of numerical density. This is because scattering expected from an organism (a krill in this case) of a given length is offset by the number of individuals required to make up 1kg of biomass. The difference in scattering per kilogram of krill biomass for krill of mean length 30mm compared to 45mm is only 1.2dB, or 32% in biomass density estimates (Lawson et. al., 2007). An alternative to this is to describe movements of layers and a measure of the importance of aggregations of a single scattering type (whether important in size or density) is to use volume backscattering in m^2/m^3. In the results section this method will be used for a discussion of the movements of layers associated with distinct scattering types and progress towards statements on the distribution of these layers in terms of biomass in the only in the "Discussion" section of this report.

One method employed to derive biomass estimates per volume sampled is to convert our acoustic data into abundance estimates per volume sampled by the average observed target strength and volume backscatter and assume a length mode from Eq.5.

$$N = 10^{(s_v - \bar{TS})} \cdot w_w \qquad (6)$$

In Eq. 7, w_w is a wet weight coefficient from literature which converts lengths to wet weight values. The biomass density is a summation of the wet weight biomass within each size class and divided by the volume sampled.

$$\rho = \frac{1}{V}\Sigma_N \, w_w(l_N) \tag{7}$$

Biomass density in the above equation is given for a random normal distribution of lengths l_N and the function converting them to wet weight $w_w(l_i)$ divided by the sampled volume obtained from the software Echoview. In order to arrive at an estimate for the density of the organisms with observable volume backscatter, it is important that they be categorized appropriately into acoustically distinct categories.

The method faces a few challenges, not least those intrinsic complications due to the large volume of integrated sample bins in potentially biologically diverse conditions. The process of acoustic classification is meant to reduce the uncertainty in the results by associating an appropriate TS model to the identified scattering region.

This is performed as an over-determined and under-determined problem. The over-determined problem is solved by estimating abundance from inversion of a series of equations (Eq. 5) based on the information for the frequency response of the estimated representative size mode of an identified dominant scattering type. The under-determined method, introduces an array of available size classes chosen from a programme of over twenty size class arrays. The inversion method can be inconsistent depending on the size classes made available, the final size range used spanned all expected size ranges for observed scatterers and matched the modes of size bins filled for the twenty different arrays. The confidence intervals for the estimates derived are given by the 95% confidence interval above and below the largest and lowest estimate. Standard error is given by the equation below:

$$S \cdot E = \frac{\sigma}{\sqrt{N}} \cdot 1.96 \quad (8)$$

In order to produce a biomass estimate it is essential to use an appropriate model within identified scattering categories to transform lengths and abundance into biomass in $g.m^{-3}$. In the context of Euphausiid-like scatterers, for example, an appropriate functional regression is the (Wiebe et. al., 1988) of:

$$w_w(L) = 5.5 \cdot 10^{-6} \times L^{3.2059} \quad (9)$$

Where, L, is the length of the organism. Alternatively, for lanternfish of the family myctophidae there is an approximate wet weight function from the Arabian Sea provided by (Karuppasamy, George, & Menon, 2008), until an alternative model may be provided for our specific area at a later date from the groundtruthing during the same cruise.

$$w_w(L) = 7.48 \cdot 10^{-6} \times L^{3.1325} \quad (10)$$

Environmental Data

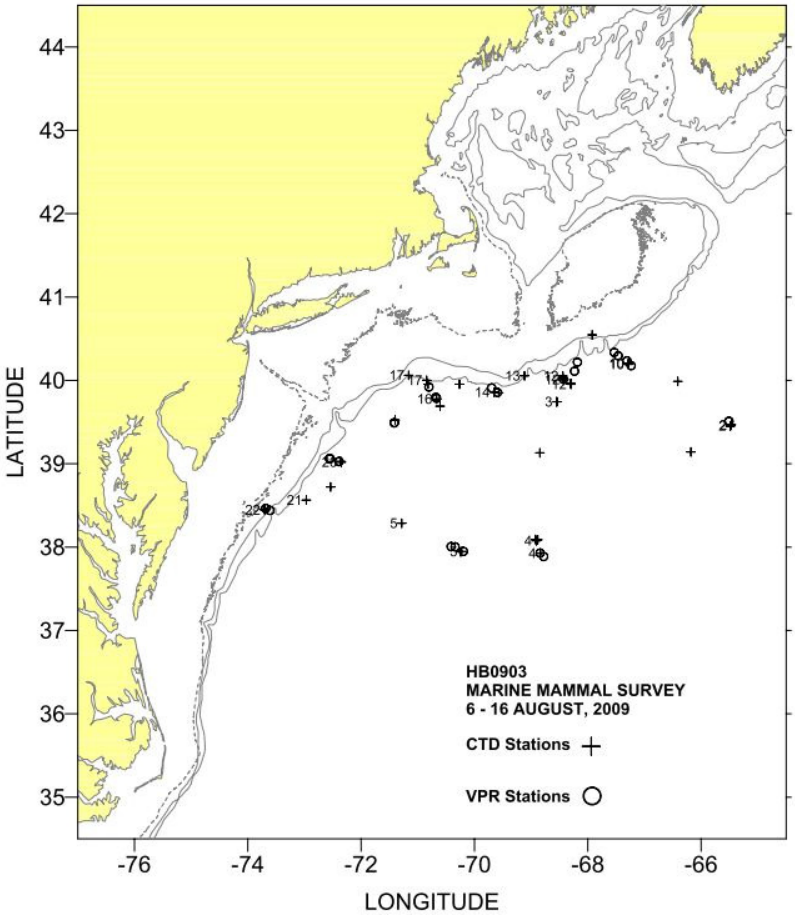

Figure 9: Map of the available CTD data from the NOAA Ship H.Bigelow 6-16 August Shakedown Cruise.(NOAA, 2009)

The acoustic data, averaged into vertical and horizontal bins along the ship's track is compared to CTD data as well as along-track surface temperature and salinity data from the ship. Furthermore, satellite data for temperature are compared with the distributions of scattering types' biomass and abundance. While the satellite data (NOAA, 2011) is more continuous over the area, thus giving a better idea of temperatures at a distance either side of the ship track, it is drawn from a data collection period that extends across the month that the boat is in the region and so statistical analysis for surface data is taken from the ship's along-track data set. The CTD data is contemporary with the course of the ship. In order to make use of this, the data is sorted into five meter depth bins, analogous to the format in

which volume backscatter will be analyzed. Data in all the given depth bins and for all integrated (~100m) blocks along the ship transect are estimated at depth along the ship's track according to a weighted method for averaging environmental data. Values for the estimation are taken from the closest data points and weighted according to the inverse distance cubed method. The inverse distance cubed method weights the contribution of each data point to the estimate according to the inverse of the distance cubed divided by the sum of weights for all data. Usually, though not necessarily, a limit is defined for the possible influence of data points (global changes to values over large distances are blocked from having any effect at all). Since the focus is in local estimation a zone of influence is limited to the ten closest data points in this method. The formula applied is:

$$\hat{v} = \sum_{i=1}^{n} \frac{\frac{1}{d_i^2} \cdot v_i}{\sum_{i=1}^{n} \frac{1}{d_i^2}} \quad , \quad \sum_{i=1}^{n} \frac{1}{d_i^2} = 1 \qquad (11)$$

Where $\hat{v}$ represents the estimate and v_i represents the exact sample data. According to this method, this should produce unbiased results, due to the weights summing to 1, as demonstrated in (Isaaks & Srivastava, 1989). The result is an echogram, of the same dimensions as the array of volume backscatter data exported from Echoview, allowing us to compare environmental factors such as temperature, salinity and density to the acoustic data to depths of 500m. While more data is available at shallower depths than at a depth of 500m due to bathymetry and CTD cast limitations, spatial variations in temperature are assumed to be less significant with depth in support of the valid interpolation of increasingly scarce data along the vessel track at depth.

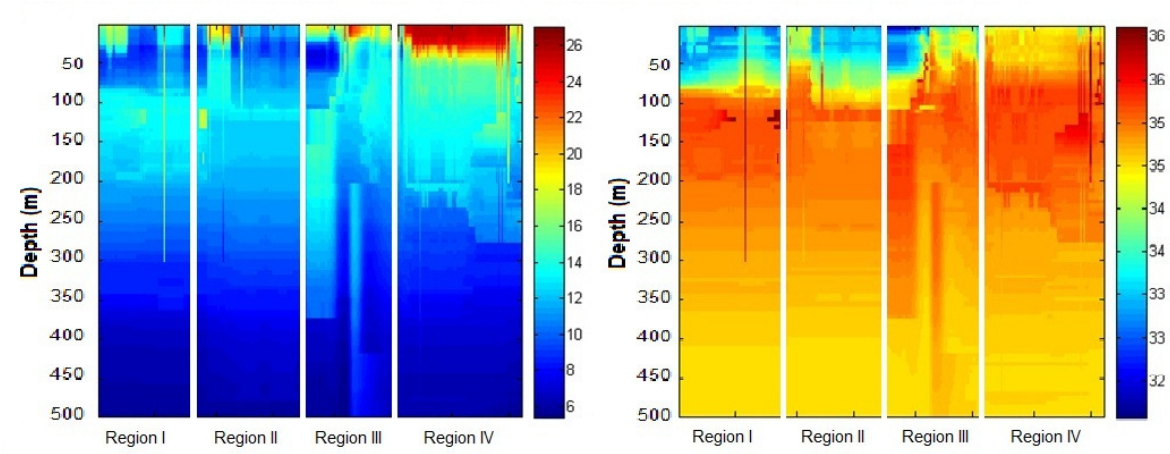

Figure 10: Along-track profile of temperature (°C), left, and salinity (psu), right. Data obtained by estimations from CTD cast data. Data for the deep water track up to 500m is given.

Defining aggregations and layers.

Aggregations were defined as continuous formations of a scattering type in the form of unbroken areas of backscatter identified acoustically as a single scattering type. This is similar to the definition presented in (Lavery et. al., 2007) as a continuation of definitions by (Barrange, 1994) and (Coetzee, 2000). Continuity was estimated visually. Similarly, while there exist very sophisticated methods for estimating layers and clusters automatically from acoustic data (Burgos & Horne, 2008), dataset in our situation was not as large or as continuous, hence results from automatically derived layer data was not as accurate as data that was determined visually. Two confounding factors have the potential to affect the results of a visual count of layers, depths of layers and thicknesses: the first is the increased beam width with depth allowing extensive patchy regions to appear as a layer if they are sufficiently clumped inside wide beam at great depth. The second is that the data will already have been integrated into ~100m by 5m bins, aggravating this effect. Nevertheless, visual scrutiny is surmised to be adequate for the purposes of this study, and, given the small size of our data present fewer opportunities for misinterpretation than automatically

identifying layer count, thicknesses and depth. The data recorded included hour of day, Longitude, Latitude, depth and thickness per layer in order to enable analysis of depth and thickness with time of day or distance from the continental shelf break.

Variables incorporated in the analysis

The backscatter coefficient (s_A), integrated over the whole depth of the water column produces a notable parallax shift from higher (s_A) in deep water to near 10dB less in the shallower region of NECS. The effect reduces as the depth of the water column increases to level around 600m depth and onwards. This is shown in Figure 11.

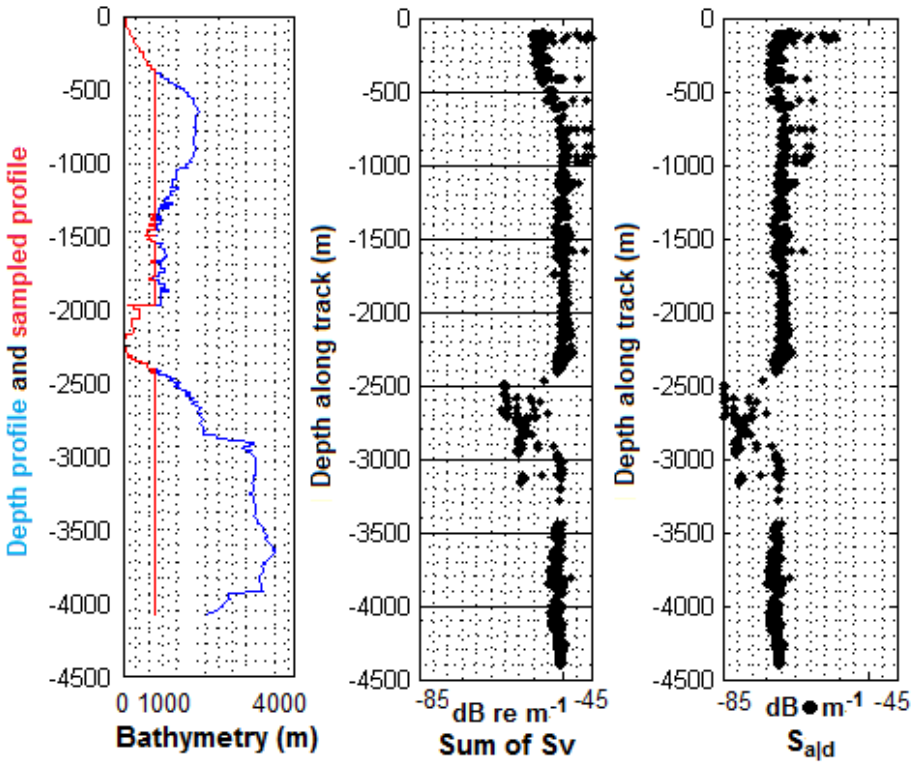

Figure 11: (s_A) for 1000m depth data at B) 38 and B) 18 kHz compared to the depth of the water column along the vessel track, and C) the same plot for depth-relative backscatter featuring no curbing of the trend in shallower waters.

This clear shift between (s_A) and ($s_{A|d}$) values spurred the definition of the NECS shelf break region as the 600m depth contour line of bathymetric data on the continental shelf. When compared with the echograms, no corresponding reduction in density of volume backscatter could be observed in the distributions observed for depth-relative volume backscatter against depth of water column. Depth-relative volume backscatter ($s_{A|d}$), is the preferred unit of reference for comparisons in horizontal distributions in order to account for the parallax introduced when observing raw (s_A) reduced simply because there is less water column. The mean of the volume backscatter in linear space will be dominated by the larger scatterers with a contribution to the backscattering orders of magnitude greater than organisms with smaller target strengths, the mean of the recorded backscatter in logarithmic space ($\tilde{s}_v$) is used to give an indication of the magnitude of scattering in the water column.

Therefore, two variables are used for characterization of the volume backscatter along the track: the mean through the water column ($\tilde{s}_v$) and the summation of volume backscattering through the water column relative to the depth of the data set giving “depth relative volume backscatter”, ($s_{A|d}$). In other words, s_A relative to a depth profile that follows the bathymetry above extent of our data, but fixed at SNR-limited depth in all regions where the bottom extends to greater depths (units dB/m). ($s_{A|d}$), ($\tilde{s}_v$) and (s_A), although comparative in value to S_v, are not intended to be directly compared to the target strength or backscatter expected for scattering types, but are used as a proxy for biomass .

($s_{A|d}$) over the whole water column tended to decrease by roughly 3dB as the depth along the track of the vessel increased from 500 to 4000m. This is a decrease that is orders of magnitude smaller than local variation over depth intervals. It is likely to be due to the definition of the variable being plotted; where more pixels of insignificant scattering can be expected in areas where the water column is deeper.

METHODOLOGY RESULTS

Acoustic Classification

Acoustic classification of scattering types consists of a series of conditions that act as filters, in order to view the variation in volume backscatter for the identified dominant scattering type. In the case of this study, acoustic samples cannot be identified from available ground-truthing but publications resulting from ground-truthing data in the area and a reference to the physical implications of acoustic frequency response can provide some clues[3].

Observed response across four frequencies

The frequency difference between each subsequent set of frequencies is given below, and reveals a very clear separation in the data between the scattering contained in the warm core ring as the DVM layer descends during daylight hours revealing a significant decrease in Sv from 18 kHz to 38 kHz. This deviates strongly from the rest of the data and correspond to similarly drastic variations at other frequency differences.

Regions of interest for ID1 were characterized by a strong decrease in scattering between 120 kHz and 200 kHz, identified in patchy structures associated with bathymetric intrusions into the top 200m of the water column and the surface interval of vertically migrating layers. ID2 was identified as scattering in the warm core ring after descent of the DVM layer and before ascent of the subsequent layer. Selections were made deliberately across thresholds of backscatter in the 18 kHz -38 kHz echogram, revealing the entire water column above the DVM layer as identifying with the ID2 scattering type without regard to Sv threshold within the region.

[3] *cf*. (Badcock & Merrett, 1975), (Backus et. al., 1968), (Stern & Serchuk, 1992), (Wiebe et. al., 1996) ...

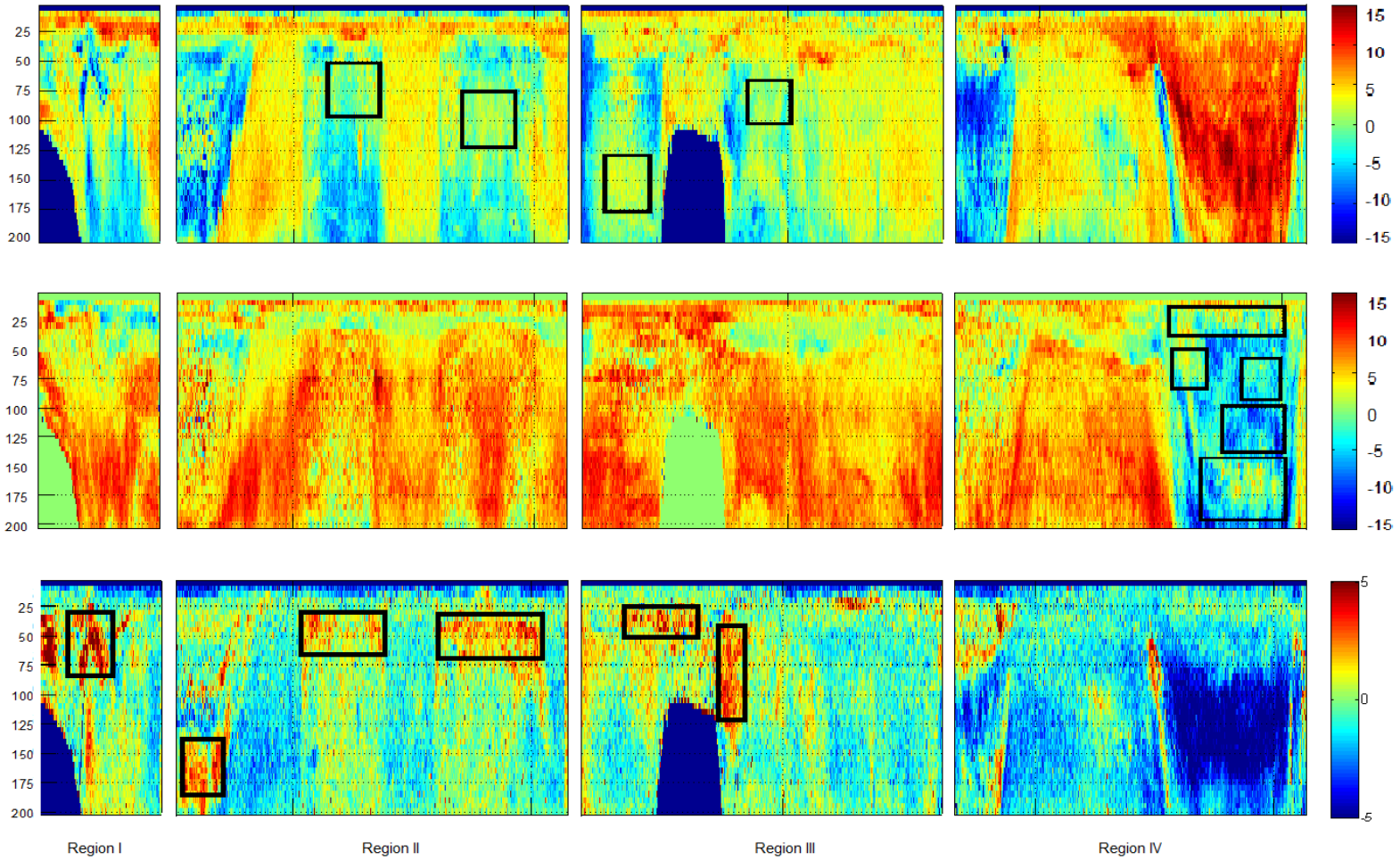

Figure 12: Mean Value Backscatter Difference (MVBD) graphs of the different frequency pairs: 38 - 18 kHz (top), 120 - 38 kHz (middle) and (200-120 kHz (bottom). The graphs show the selection loci for ID5 (top), ID2 (middle) and ID1 (bottom).

ID5 was identified by regions showing a moderate decrease in relative backscatter and occurring below the ascended layer at depths between 75 and 150m. Samples for ID3, in the ascending and descending layers showed a reduced level of backscattering difference compared with ID5. ID4 was selected from patchy distributions ascending slowly in the hours preceding the dominant DVM cycle. Each region is sampled by 150 random points such that the frequency response of each data is traced to produce a mean frequency response with associated error margins and the differential of the frequency response which is analogous to the filters applied for acoustic classification. ID6 was input as a filter to search for what is commonly accepted as euphausiid-like backscatter within the sample. At this stage all distinguishable scattering types, given that they come from regions identified from the structure available to us in the echogram, are maintained separate regardless of potential identity.

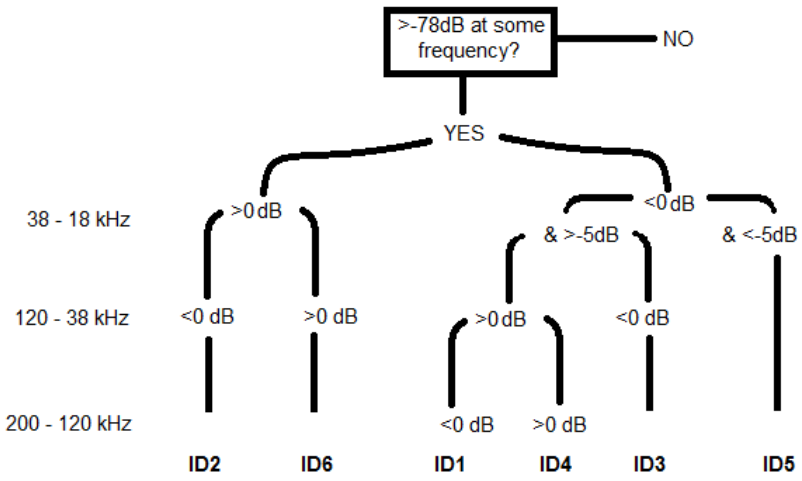

Figure 13: Illustration of the classification method used to ascribe acoustic identities

Bimodal distributions emerge at all frequencies, the principal modes occur between [-80, -78] dB and [-78, -70] dB for data at the lower frequencies and between [-90, -81] dB and [-81, -70] dB for data at the higher frequencies. This was found not to separate the data into

separate scattering types, but to resolve between areas associated with low Sv at the outer edge of scattering identified as coming from a biological source. Much of the identified backscatter from these lower modes occurs below 700m where noise potentially becomes a significant issue on the 38kHz data, and does not produce additional structure within the low backscattering regions when higher scattering is removed by a threshold.

By applying the filters to the data based on observable and consistent frequency responses within our data set it is possible to track the migration and distribution of different scattering types through the water column that reveal separations and associations between scattering types. The well defined difference between regions identified as ID2 within the warm core during daylight hours is still evident. A layer of ID3 is seen to descend in parallel with the DVM layer, within the region identified as ID2 and settles in a patchy distribution to 150m depth. Also interesting is the close association between ID5 and ID3 despite being consistently distinguishable by their frequency response and forming reasonable scattering structures in agreement with the raw data which lends credibility to them being categorized seperately. The samples captured along with those scatterers belonging to ID5, look as though they may belong to ID1 and ID3. Furthermore, if a region does not backscatter at above -78dB at any of the four frequencies their frequency is not classified. IDs 4 and 6 were taken from regularly appearing patchy swarms of low scattering at 120 kHz and 200 kHz.

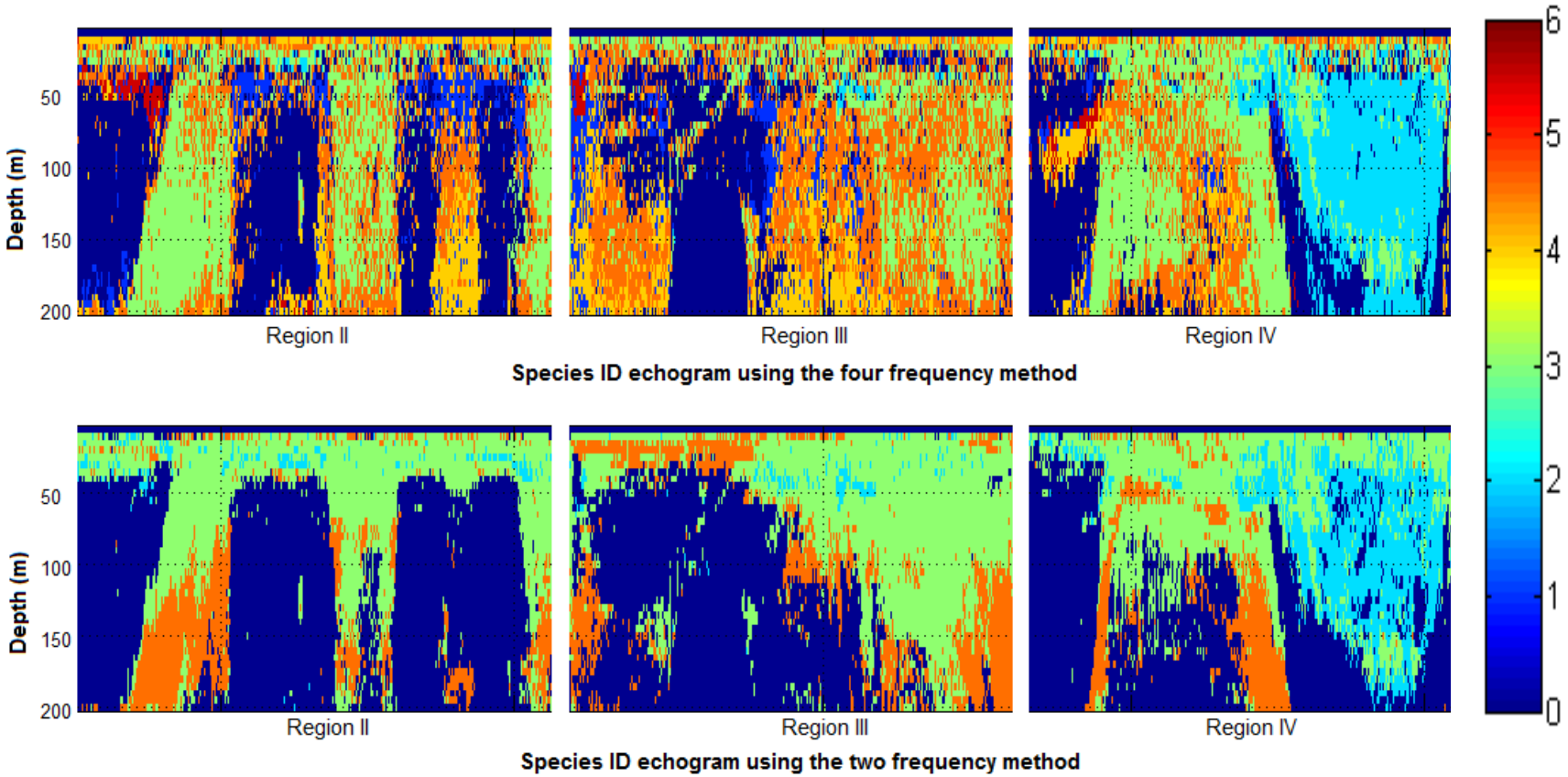

Figure 14: Comparison of the identified species-ID echograms for the four-frequency method (above) and the two-frequency method (below). ID2 = cyan, ID3=green, ID5 = orange, ID6=red, ID4=yellow, ID1 = 1. (ID4 and ID6 are incorporated into ID3 in the two-frequency method.

Searching for information within the data

This study looked at two possibilities for identifying taxonomic groups using two frequencies. The first was an attempt to reduce the indeterminacy of the problem of acoustic classification over two frequencies, by exploring additional information, including thresholds and statistical parameters for the local variations in the original data contained within 5m by ~100m blocks, such as kurtosis, skewness, variance and separating out the probability distribution function of volume backscatter by thresholding. The second relied on simply accepting reduced resolution from our 200m taxa identification algorithm and basing the IDs beyond that depth on the two frequency method between 18 kHz and 38 kHz and resolving for three groups comprising ID2&6, ID5 and IDs3,1&4 respectively.

Variation of Statistical parameters within 5m by 10 ping integrated blocks

The data set, at original resolution with, was re-sampled into bins corresponding to the data used in our analysis and analyzed for the possible use of kurtosis, skewness and variance as an indicator of species ID. The results for kurtosis yielded no obvious structure, while variance was coincident with the regions with dense variance of acoustic frequency responses. This highlights agglomerations of different scattering types near and above bathymetric features such as seamounts and the shelf break as well as in the surface layer and immediately surrounding the ascending and descending layers. Variance in the surface layer decreases at the bathymetric feature where a migration away from the surface starts, and also decreases at the arrival of a migrating layer from deep waters. This marks the arrival and departure of dominant scatterers, either by virtue of their acoustic strength, resonance or biomass, capable of overwhelming the other signals.

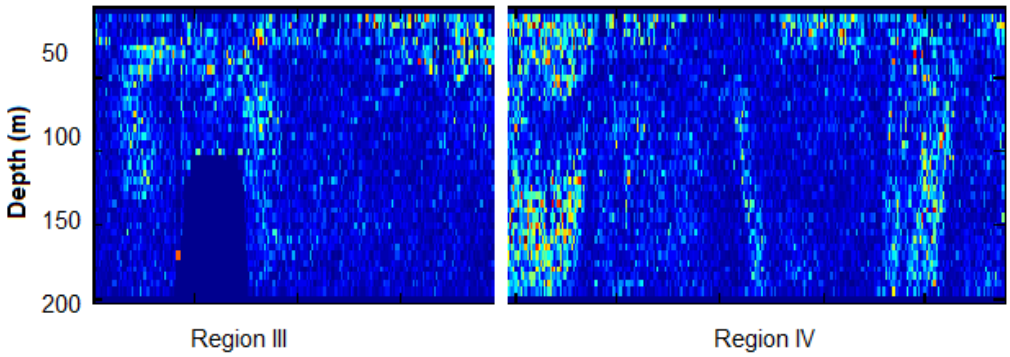

Figure 15: image of variance of samples within 5m by 100m integrated blocks for the data set, where low variance in dark blue increases to higher variance in through green, yellow and red.

Identification across two frequencies

A two frequency method can then by developed to discriminate between IDs 2 and 6; ID5 and IDs 3,1,4. If there is no variation between 18 kHz and 38 kHz the data is deleted. If δMVBA exceeds -6.5dB and the raw scattering exceeds -78dB then the pixel is classified as ID5. In the event that scattering is again greater at 38kHz and above -78dB, but MVBD is inferior to 6.5dB in magnitude, then the method classifies as ID3 containing IDs 3,1 & 4 from the top 200m method. Finally, IDs 6 & 2 are stronger scatterers at 18 kHz who backscatter at above the threshold of -78dB.

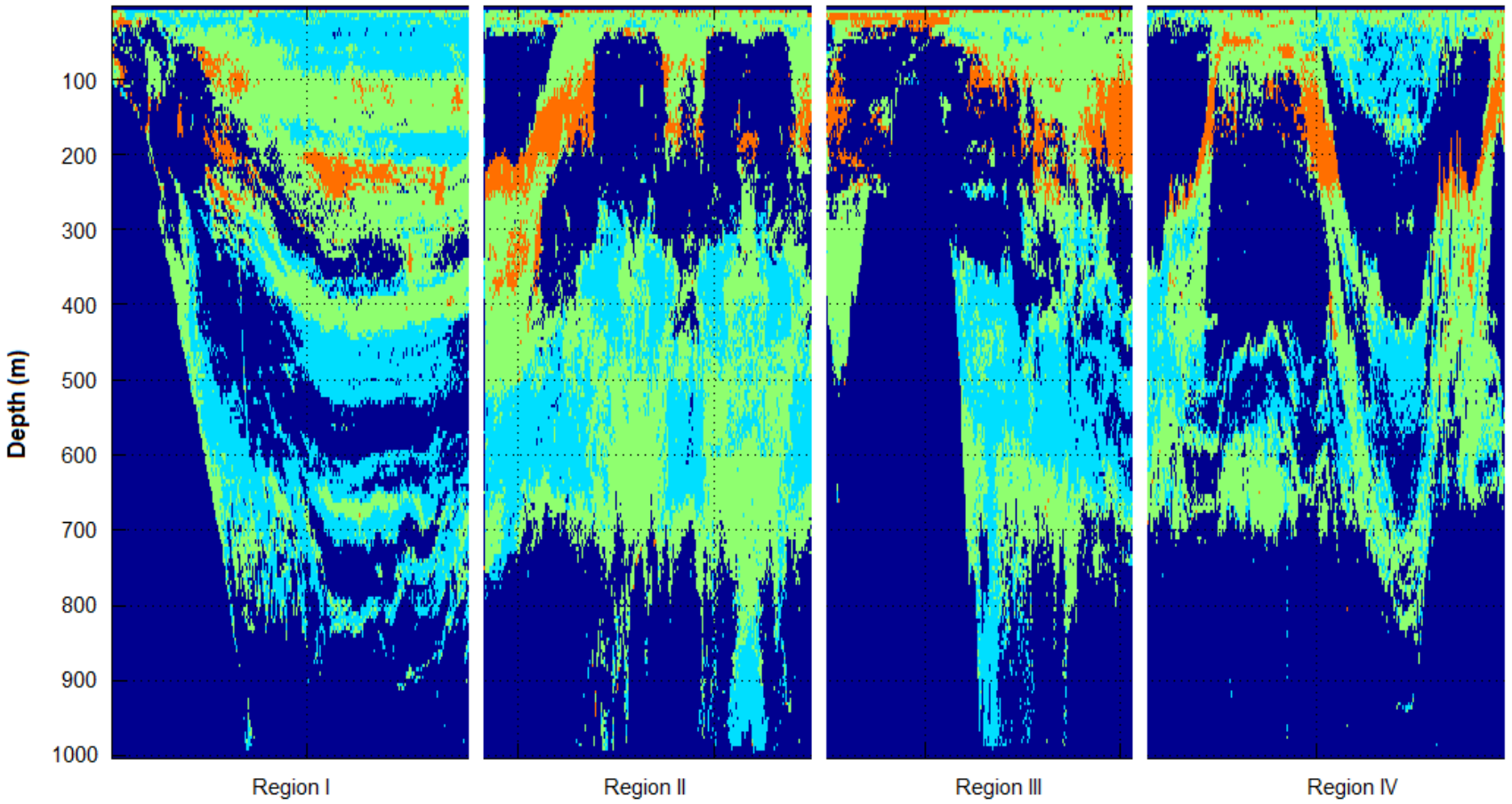

Figure 16: Categories of ID passed through to the full depth echogram. ID2 = cyan, ID3=green, ID5 = orange

Although the match is far from a mirror image, the key variations remain the same. ID3 remains the dominant scatterer for the deep migrating phases, and continues to be important at depth below the ascended layer. ID2 remains similar, present predominantly in the warm core ring after descent. ID5 varies much more from the two-frequency method but tends to be associated with ID3 in the same way as it did by the four-frequency method and occurs below the ascending and descending layers as expected. Furthermore, the slope between 18 kHz and 38 kHz has implications for the likely size of scattering elements, where a steeper slope indicates increased proximity to the resonant frequency of the swimbladder implying a smaller size of swimbladder and suggesting a smaller size of scatterer.

A randomly generated set of coordinate points is selected from a particular ID that is identified by the two frequency method. These coordinate points are used to run though the coordinates of all points attributed to the same ID by the four-frequency method. If the dominant scatterer, within a 3x5 pixel (15m by 500m) frame and the ID determined by the two-frequency method are the same, a success or “1” is recorded for that random point, otherwise a zero is recorded. The confidence in the accuracy of the two-frequency method in correctly identifying the four-frequency ID using the two-frequency ID is interpreted as the success rate. This operation is repeated for increasing numbers of randomly generated points. Results are summarized in the figure below:

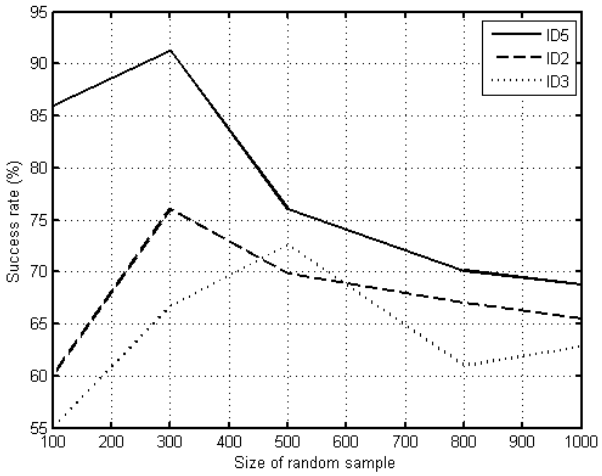

Figure 17: Percentage success rates for increasing numbers of randomly generated indices within a scattering type.

The results of the two frequency test suggest that if we are to repeatedly pick points at random within the two frequency method and compare them to data classified according to the four frequency method, the success rate would eventually settle somewhere between 60% and 70% accuracy. The echogram below shows a direct comparison of such an experiment for the top 200m of the water column. At 65% accuracy this provides a way of at least reducing the variations between regions of volume backscatter in order to allow the analysis to penetrate beyond 200m, even if the higher frequencies don't. Without considering the ability for the identification method to distinguish between ID3 and ID5, this method still resolves regions of greatest scattering at 38kHz (ID2) in contrast with the regions of greatest scattering at 18 kHz while removing backscatter not exceeding -78dB at any frequency.

RESULTS

This section looks at volume backscattering over the vessel track and addresses variation of total backscattering and backscatter at given depth intervals over the time of day, the track of the ship relative to the distance from the New England shelf break and in relation to other environmental data (Temperature and Salinity). Acoustic data are analyzed for the water column to a maximum of 1000m depth at 18 and 38 kHz as well as data for the water column down to 200m at 18, 38, 120 and 200 kHz.

Whilst actual classification of backscatter is postponed for the discussion section of this paper, the descriptions of the distribution and migration of volume backscattering at lower frequencies should be more relevant to scattering types bearing gas bladders, whilst those descriptions at higher frequencies would be more relevant to bladderless scattering types. This natural thresholding can be considered a first method of acoustic classification.

Results at 38kHz

The data collected revealed high values and range of depth-relative volume backscatter ($s_{A|d}$) in warm waters (25°C temperatures) (6 to 10 dB higher than other areas), defining these areas as a biologically special zone of interest. The section of track in question, Region IV, (Figure 4) as the boat crosses over the continental slope at its farthest extent from the New England shelf break and passes through a body of warm water [37.5N to 39N and 65W to 71W], as described in Figure 18 below. Considering the top 250m of the water column, where there is data over a longer track, there is a second 'hot spot' corresponding to Region VI, Figure 29, and corresponding to the section of high ($s_{A|d}$) as the vessel passes over a slender body of warm water extending out of the warmer core.

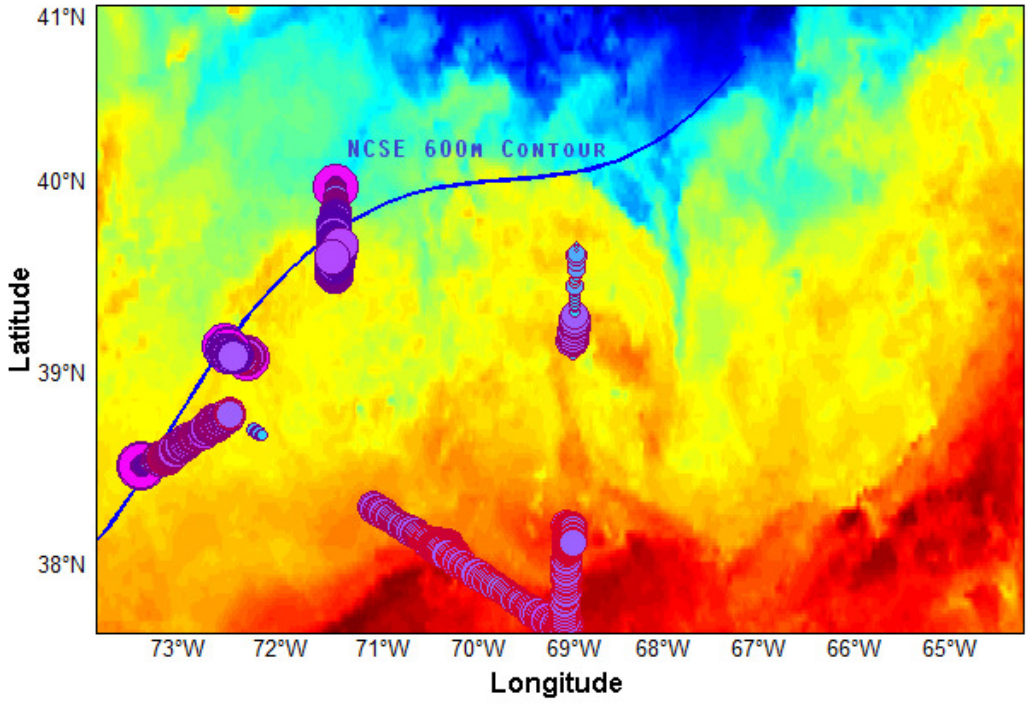

Figure 18: Vessel track analyzed plotted over the sea surface temperature (°C) data from NOAA, 6th-16th August 2009. Increase in depth integrated ($s_{A|d}$) is given by increase in seize of marker between -70 and -40 dB re m-1

The areas of high ($s_{A|d}$) off the shelf break are coincident with a temperature mode as illustrated in Figure 9. Considering the environmental data acquired at depth over the track of the cruise, observations of high ($s_{A|d}$) also correspond to distinct variations in the structure of salinity data with depth (Figure 10).

While the sum and range of ($s_{A|d}$) increases at the 25°C temperature mode, the salinity profile show regions of enhanced mixing over the water column, Figure 10. The DVM pattern illustrates synchronous ascents and dispersed descents within the NECS shelf break region but more symmetrically synchronous DVM patterns within water associated with higher temperatures in the warm core ring region. The ascending layer breaks up into a broad spread of patchiness and layers extending from the surface down to 150m, although a region of intense scattering (greater than -68dB) is restricted to the top 50m of the water column near the shelf break region and extends just over 100m in the warm core ring. Veiwing the

evolution of data at constant depth pair-wise with the environmental data set allows some insight into the mechanism and depth-structure associated with this region. The graphs below look at ($S_{A|d}$) as it varies with environmental data.

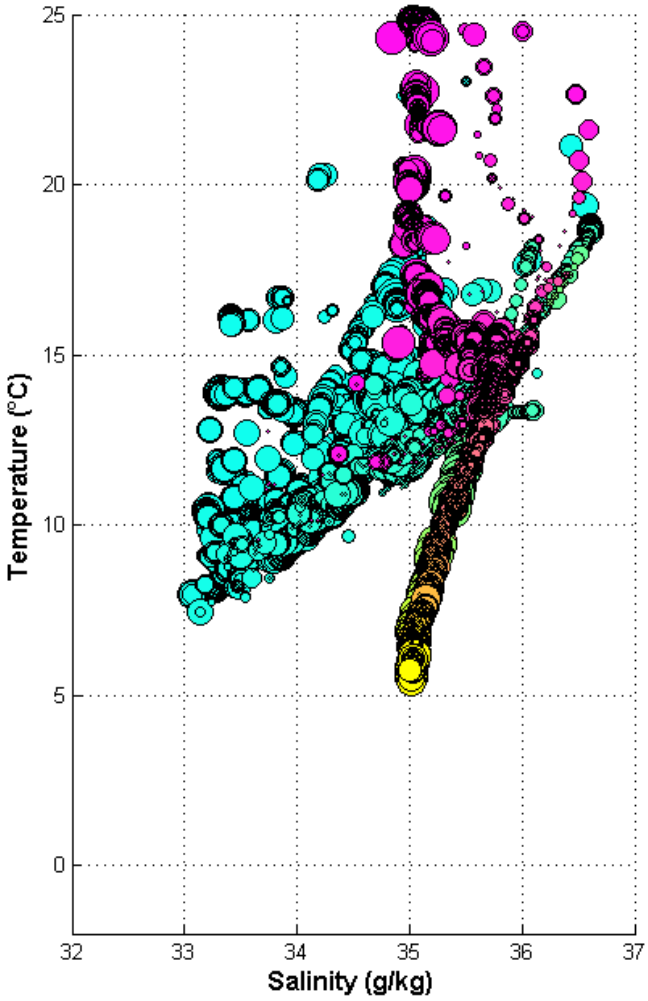

Figure 19: Temperature and salinity paired with volume backscatter density; data to 500m at 18kHz. The size of data points represent variations in volume backscatter between –80 to -60 dB and depth increases as data points become yellow in colour.

Figure 19 shows the distribution of (Sv) in the various water bodies characterized by temperature and salinity. There is increased backscatter in regions of high temperature (cf. Figure 25). The bodies of water observable over the shelf are clearly distinguished from those. This observation, along with the coincidence of surface temperature and salinity

anomalies throughout the water column, suggests that the structure of temperature and salinity data observed at the surface also has bearings for organisms at depth. The greatest range and magnitude of ($s_{A|d}$) at a given depth of the bathymetry occurs nearer the surface upwards of 300m and represents a variation in expected volume-integrated backscatter three times greater than in the rest of the water column.

The contiguity of layers from the surface to layers at depth shows the importance of mesopelagic layers' contribution to the biomass observed in the top 200m of the water column.

The 200m depth ($s_{A|d}$) data seems to fall around 0 - 3dB lower than the mean values from the track with data down to 1000m. This is indicative of a distribution of backscatter that tends to be concentrated at the surface, in accordance with the sampling bias, with deeper layers contributing roughly half the total volume backscatter. This is not to say that the contribution of meso-pelagic organisms is insignificant in our data set, since most of our data occurs at night, with the rise of meso-pelagic scattering layers from 200 to 1000m depth to the surface. The "patchiness" of observed backscattering in the top layers is partially induced by the very nature of potential scatterers encountered at the surface, but also due to the narrower insonified area at shallower depths, closer to the transducers. The increased variability of Sv values and patchiness in the surface layers at night for higher frequency data is attributed to predominant resonance at the lower frequencies.

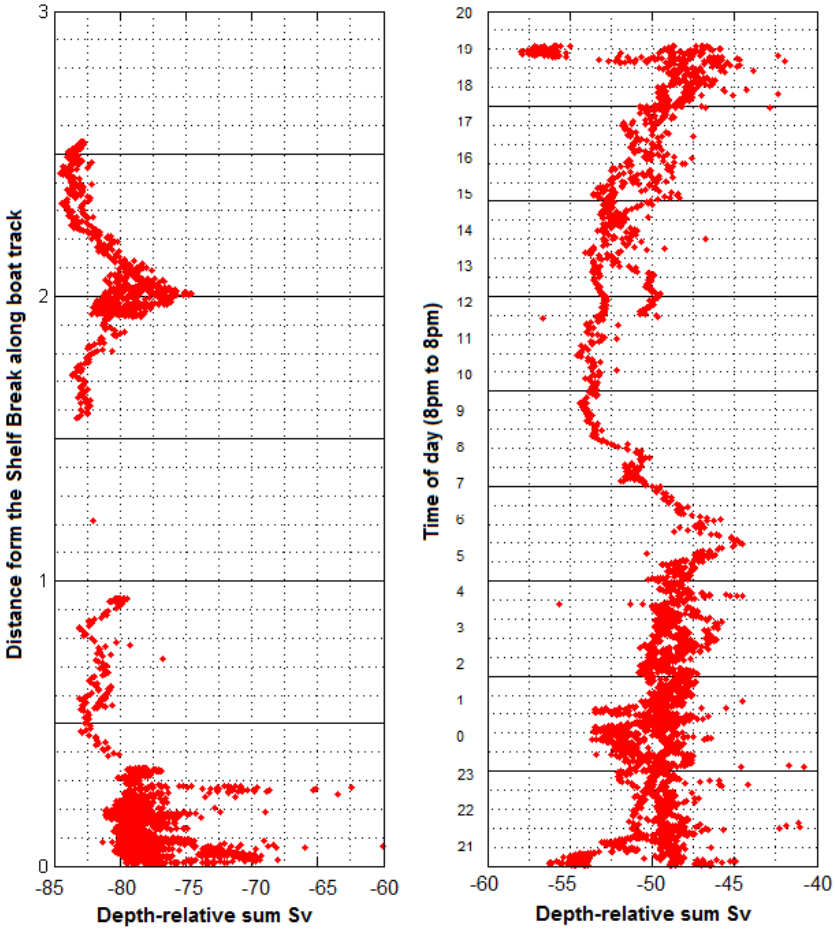

Figure 20: Depth-relative volume backscatter varying with distance from the NECS (Left) and Depth-relative volume backscatter with time of day (Right).

The figure above, reveals more clearly the much stronger scattering near and just off the New England shelf break region as compared to the alternative area of high ($s_{A|d}$) which coincides with the warm core ring. The waters in between these two areas show a considerable drop in depth-integrated volume backscatter. The right hand graph of Figure 20 shows a dramatic drop in ($s_{A|d}$) at 0800hrs which slowly recuperates to midnight levels from 2030hrs onwards. This coincides with diel vertical migration ascent and shows a more relaxed timing and reduced synchrony on the descent. timing and implies an increase in

density as organisms come together in the surface layers followed by a decrease as they settle out to varying depths in the water column in the daylight hours.

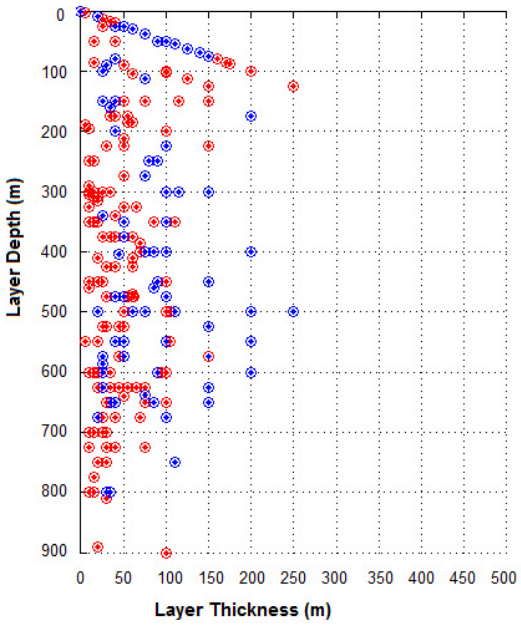

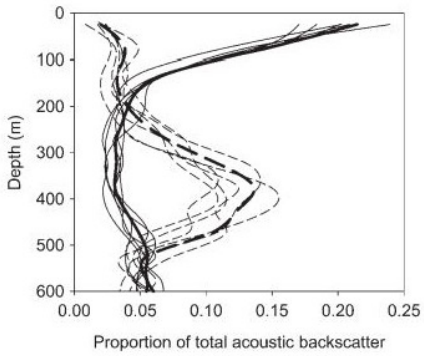

Figure 3. Vertical distribution of total acoustic backscatter integrated in 50 m depth bins on the Chatham Rise observed during the day (dashed lines) and at night (solid lines) in 2001–2007. Thin lines show data from individual years. Thick lines are averages over the 6 years.

Figure 21: Thickness and depth of scattering layers obtained from visual inspection at 10m by 100m bins in the track; data for data at 18kHz and 38 kHz; Data occurring between 2100hrs and 0400 hrs is marked in red and data occurring between 0600hrs and 1900hrs is given in blue. These day and night distributions compare well with (O'Driscoll, Gauthier, & Devine, 2009).

The thickest layers seem to form between 200 and 600m. Thicker in the upper 600m tend to be either 20 (principal mode), 50 or 100m thick. Layers between 600 and 1000m tend to be much thinner. The layer thickness principal mode of 20m is present throughout the water column; the depth range between 200 and 500m seems to differ only in that a proportion of the occurring layers can reach thicknesses up to 250m, where the most layers reach a maximum of 150m thickness. This is in good agreement with the distributions observed in (O'Driscoll, Gauthier, & Devine, 2009) for night and day distributions of mesopelagic fishes.

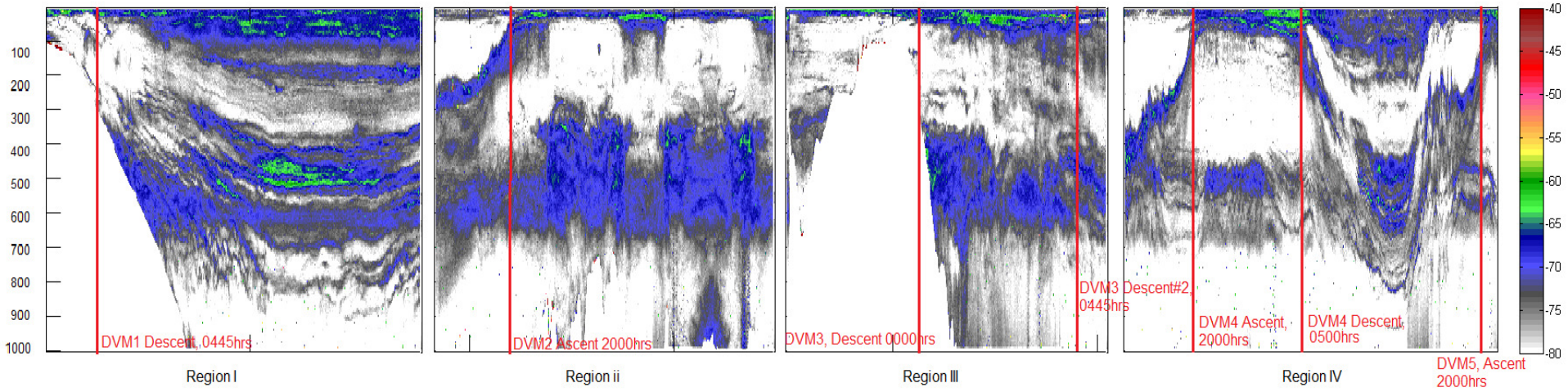

Figure 22: Image of the echogram at 18kHz detailing the observed dial migration patterns over the first four regions of the NECS data.

A deep non-migrating layer at 700m oscillates through 100m over the day while a surface non-migrating layer constrained to the top 50m of the water column is joined by the dominant DVM layer at 2030hrs, leaving between 0200hrs and 0400hrs in the shelf break region, but staying until 0440hrs during the DVM cycle associated with the warm core ring. The descending layer on the shelf break region scatters more strongly and forms four layers (40m, 250m, 400m and 500m) at shallower depths than those observed in the warm core ring, though some faint scattering is still observed at depths similar to those observed within the warm core ring. Within the warm core ring a layer forms at 150m, with a larger "void" until the next one at 475m and 750m. Diurnal events in August were recorded at between 0420hrs and 0445hrs for sunrise and 2028hrs and 2041hrs for sunset; real noon was between 1541hrs and 1631hrs.

The deep migrating layers near the shelf break migrate together from 200m onwards, covering 150m together at an average rate of 3.6 to 4.5 m/min. In the warm core ring the two deeper layers come together circa 250m and cover 230m together at an average rate of 2.1 to 2.8 m/min. The shallow, patchy, migrating layer ascends at 0.2 ± 0.1 m/min on the shelf break region and 0.4 ± 0.1 m/min in the warm core ring water. Speeds are symmetrical within the warm core ring, but it is difficult to determine a comparative speed for the shelf break, though it shows clear asymmetry in its descent phase. An analysis of 3 DVM cycles in the warm core ring, and 4 DVM cycles on the shelf break available at 120 kHz showed that both layers inside the warm core ring and on the shelf break have separation of layers as they reach the surface – some rising fast above the main DVM layer at 5 to 6 m/min in either ecosystem, others maintaining a nearly horizontal track at around 150m depth. The warm core ascent also seems to present two separate rates in its ascent ranging from 1.4 to 2.05 m/min before the rapidly ascending layer splits off and accelerating to between 1.57 and 2.8

m/min after that. Descents were difficult to assess for the shelf ridge system but could be roughly approximated at 2 m/min prior to the descent of the trailing edge and 7 m/min at the trailing edge. The warm core ring DVM layers were 2.1 to 2.8 over the ascent and descended at 3.6 to 4.2m/min. At DVM1 a descending layer is intercepted as the boat moves offshore.

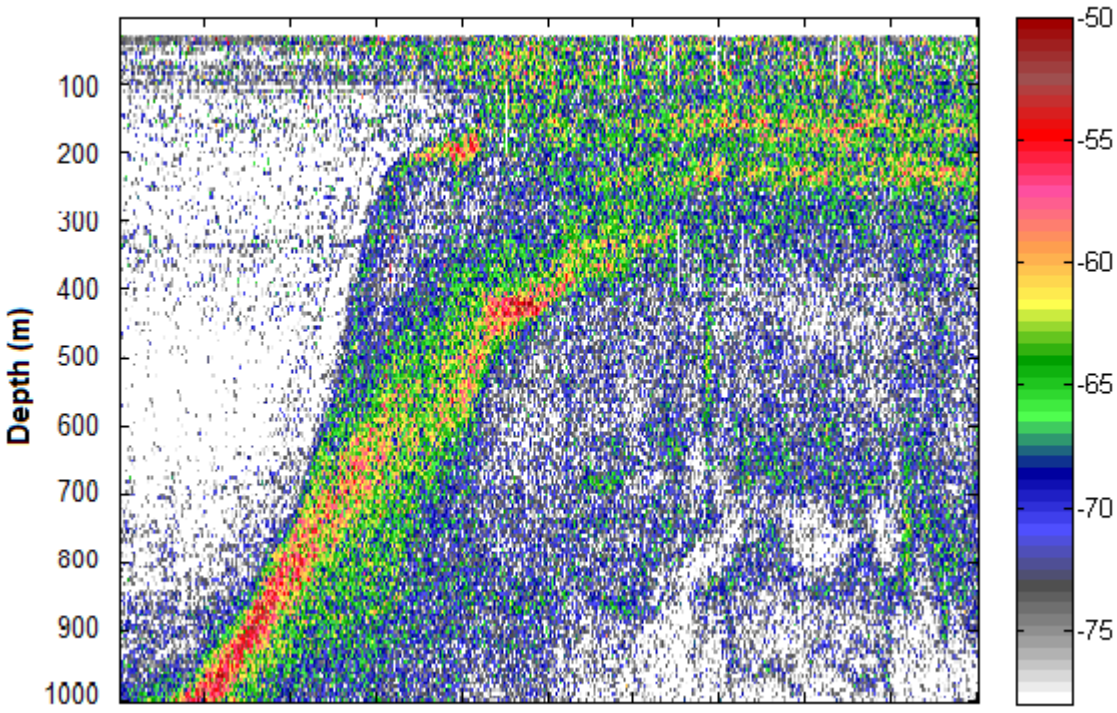

Figure 23: Close-up detail of a typical ascending layer, both in the warm core ring and on the shelf, as scattering seperates out by speed of ascent and behaviour. Threshold is set to -80dB.

Identifying distinct populations by frequency response over 18 kHz and 38 kHz data

Figure 24 shows example locations in the echogram where it is not possible to distinguish populations by their frequency response (18 to 38 kHz), top, where populations are similar but divergence in identity can be argued, middle, and where populations are clearly

separate, bottom. The plots are based on a random sample of 100 points from the identified regions. These comparisons are possible since there are no incidences showing resolved scatterers in the data set. This avoids any situations where an intense scatterer would appear as a small region of -50dB surrounded by background-strength scattering at a shallow depth, and the same scatterer averaged over a larger volume would appear as -60dB at depth. The uppermost graphic of Figure 24 describes the distribution for two areas that backscatter more strongly at 38kHz than at 18kHz. The two *adjacent* regions are connected continuously though the vertical change in structure is likely to be a spatial one, not induced by a phenomenon of migration, but rather as a result of the boat turning acutely. The question is whether these scatterers are the same, or at least the same mix of scatterers? Both spread along the line of zero dB-difference, though the range of scattering for zone 1 is less and its variance greater than zone 2. The resulting plot of Sv at 18kHz on 38kHz Sv is not convincing either way. The second graphic shows a little more clearly that two, disconnected and *depth-seperated*, populations each having small or absent swimbladders are more likely to represent different scattering types than in the previous example. Considering two completely different zones, one from each scattering type, there is a clear separation of the samples and this should not be a surprise but helps to illustrate the ranges of variability to expect. In this way, the initial classification then becomes a guide enabling further sampling and characterisation within each scattering type, which will be used to compare the DVM layers in the discussion section.

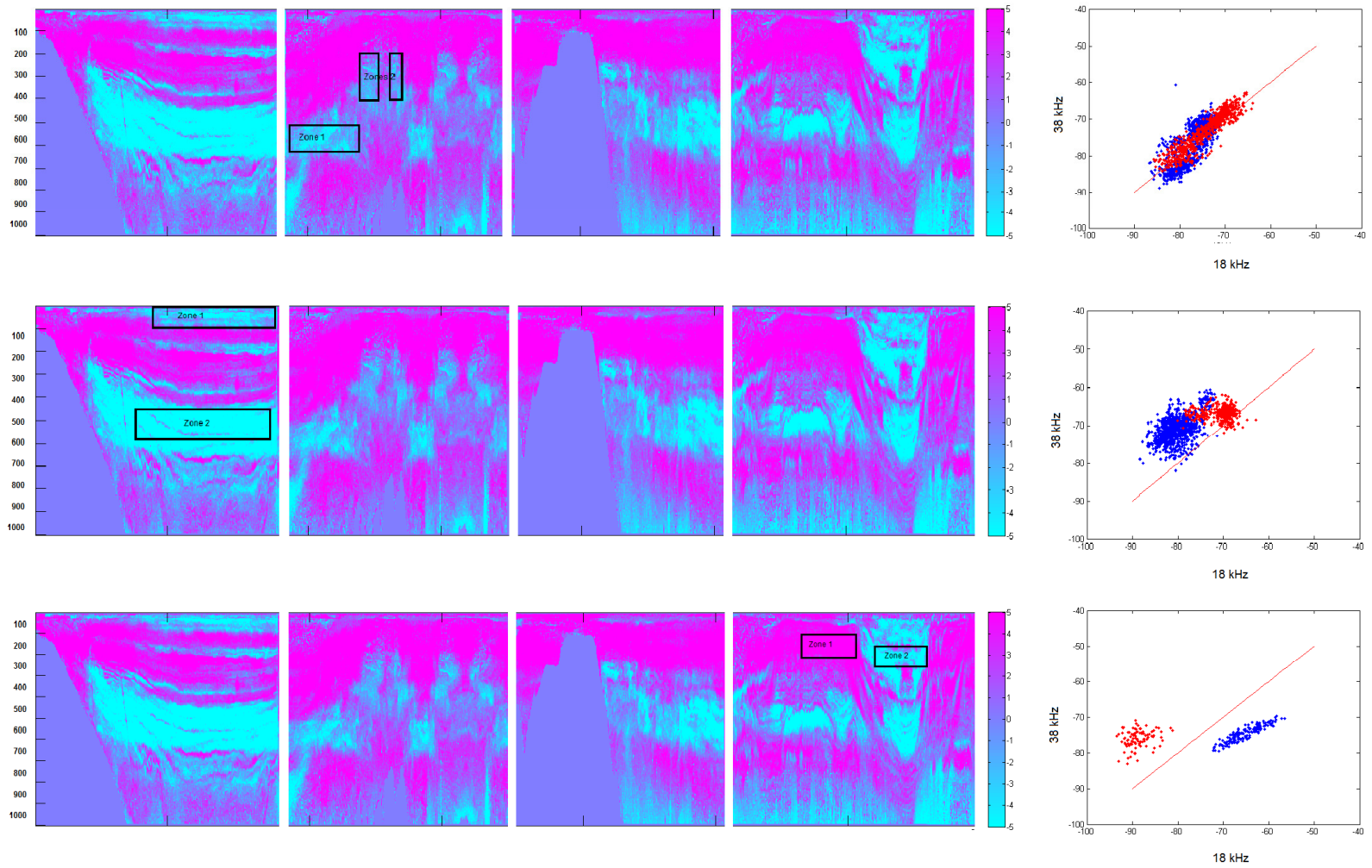

Figure 24: Scatter plots for the distributions of different regions over 18kHz and 38kHz describing situations of clearly distinct scattering types or looking at samples from similar scattering types and other situations where it is much more difficult to determine the distinctness of scattering types. Zone 1 is presented in blue on the scatterplot, and Zone 2 in red. The echograms show MVBD echograms between 38 kHz and 18 kHz; cyan colors indicate higher scattering at 38 kHz, mauve colors indicate higher scattering at 18 kHz.

DISCUSSION

The data over the NECS region is representative, at the scale of the basin, of relative distribution and migration patterns for epipelagic and mesopelagic organisms as they are defined on the shelf break region as compared to nutrient-poor continental slope waters and within the warm core ring.

The purpose of this discussion is to define and describe the characteristic variations of each region within the data set. An attempt is made to argue for the identification for scattering types separated out by two and four-frequency species identification methods, in coordination with the environmental data. The identification will be used to support a thesis on appropriate TS-models in order to come to estimates of biomass per meter cubed and length estimates.

Horizontal distributions vary with depth

Patterns in presence or absence of strong scattering at 18 kHz over the region seem to be determined by position. This does not however limit them to being a product of bathymetry, since the rates at which the warm core rings migrate is much slower than the course and passage of the ship over the 10 days (Endo & Wiebe, 2004)(Mann & Lazier, 1996). Mann & Lazier state that warm-core rings have mechanisms for generating upwelling of nutrient-rich water especially near the perimeter in the high-velocity zone. We expect to find greater levels of primary production in the rings than in the surrounding slope waters and subsequent growth through the trophic chain. The intriguing matter regarding these structures is that some meso-pelagic organisms remain exclusively within the warm-core ring and can be traced acoustically throughout its life, with no significant evidence of change in

abundance or vertical distribution (Mann & Lazier, 1996). This phenomenon could explain the coincidence of high levels of ($s_{A|d}$) and the surge of salinity levels characteristic of deeper layers up through the water column to meet the hotspots of 25°C water (cf. Figure 10).

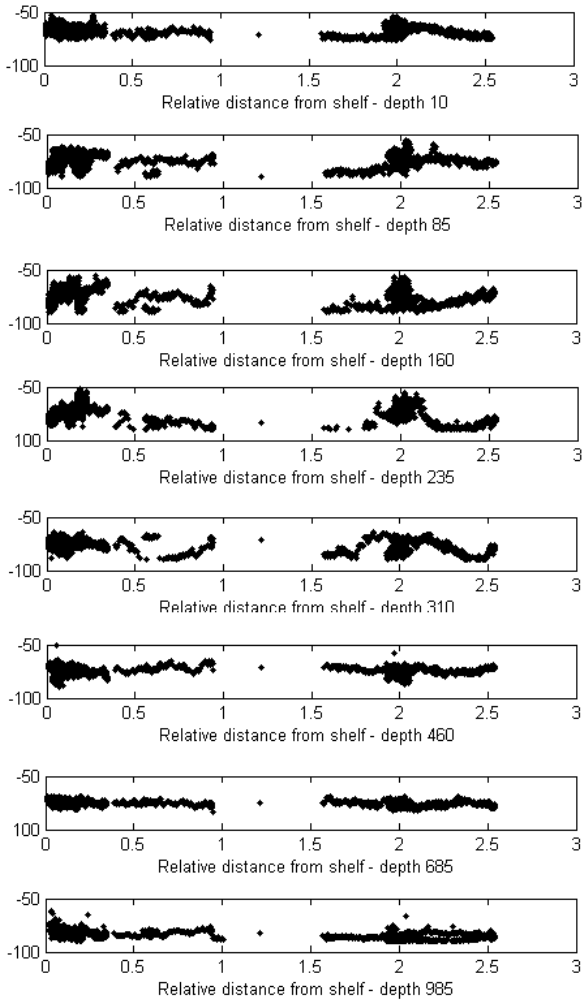

Figure 25: Volume backscatter density as it varies with distance from the GBK shelf region for different depth layers.

Distinct Biological composition of the warm core ring

With reference to the method used in "Identifying distinct populations by frequency response over 18 kHz and 38 kHz data", a significant shift in pattern emerges between the regions of DVM near the shelf and within the warm core ring. Samples of 100 points are

taken from the dominant migrating layer during its ascent, surface interval in the top 50m of the water column and from the non-migrating layer.

Clear trends can be seen; both ascent and surface regions show scattering that is stretched along the Sv_{18kHz}=Sv_{38kHz} line, showing high variability in Sv values in the range [-74 -57]dB. There is a significant separation between the means and variance of the migrating and non-migrant layers (>10dB), suggesting that this difference is somehow reflected in the acoustic properties of the organisms and hence by their anatomy or behaviour. The migrating layers show MVBS differences of ranges [-2 -12] and [8 -12] dB respectively for the ascent in DVM2 and DVM4. Both surface interval regions in each DVM show variations of range [3 -7] and [3 -10]dB. Between the two observed migrations the one centred on the warm core ring exhibits on average 2dB higher mean Sv over both frequencies and all three samples as compared to the DVM observed over the continental slope. In both situations the scattering observed during the ascent and over the surface interval distinguishes itself as near mutually exclusive to the scattering observed as a tight cluster of points scattering more strongly at 38kHz than at 18kHz – another contrast to the scattering in the migrating layers. This is not unexpected physiologically, as non-migrating deepwater organisms would tend to fill their bladders with lipids, instead of air, over the course of their life history or will not have a swimbladder at all (Catul et. al., 2011). Thus a similar scenario is observed over the continental slope as within the warm core ring but revealing differences as well. The distributions observed within the warm core ring present significantly different variance and means from the shelf break.

This suggests that the warm core ring supports biologically diverse life with respect to that which is observed over the shelf and supporting (Mann & Lazier, 1996)'s description of the warm core ring as a biologically separate ecosystem.

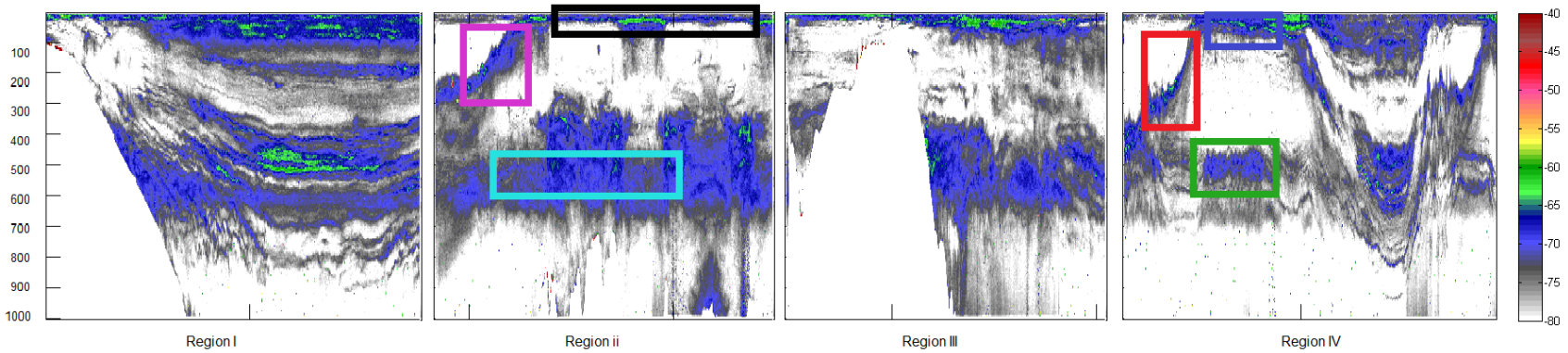

Figure 26: Regions for relative frequency response variability study. Region 1 in blue, Region 2 in red, Region 3 in Green, Region 4 in Mauve, Region 5 in black and Region 6 in cyan.

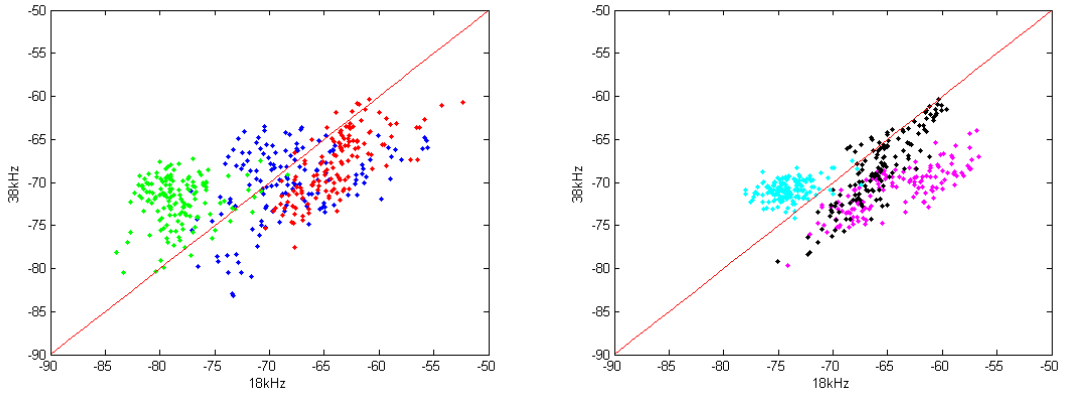

Figure 27: Relative frequency response of regions 1 to 3 in figure (Left) and Regions 4 to 6 in figure (Right). Regions 1 and 4 describe the DVM ascent, Regions 2 and 5 describe the top 50m of water at night, and Regions 3 and 6 describe the non-migrating layer.

Identifying Acoustic Scattering Types

The two methods, as our most accurate method for distinguishing different types of scattering organisms, results in the scattering types identified in the figure below. The species-ID echogramme of these acoustic scattering types in the top 200m of the water column was incapable of showing that the organisms within the dominant DVM layer of the warm core ring were separate organisms. This resulting scattering types nevertheless allow us to move ahead with associating a TS-model to the acoustically distinguishable scattering types and making abundance and biomass estimates. This is possible because, while the frequency response may not be species specific it will give coarse, though crucial, information on the physical properties and general size of acoustic scatterers.

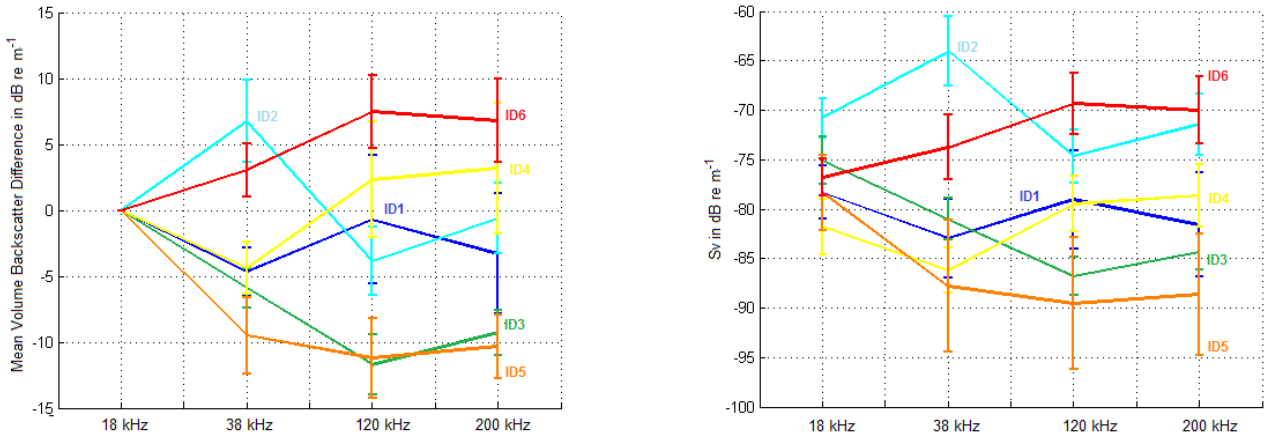

Figure 28: Graphs of the relative frequency response (left) and the mean-value back-scattering difference for samples at each frequency pair (right) for Acoustic scattering types 1 through 6. cf. Figure 14 for color coding.

IDs 3 and 5 are contiguous although there is clearly a difference in general strength of backscatter across all frequencies between them. Both have a similar decreasing frequency response between 18 kHz to 200 kHz and their error bars overlap. This kind of scattering implies the presence of a gas inclusion and the steeper slope for ID5 implies that this gas inclusion has a smaller size, generally. This includes a range of organisms including all swimbladdered fish, siphonophores and some jelly

fish. The layering evident in our data set as well as observed swimming speeds support the thesis that the dominant scatterers for IDs 3 and 5 can be modeled as fish for biomass estimates. The ratio of swimbladder to standard length varies significantly between fish species but it is common for the size of the bladder to correlate with an increase in the fish' biomass, although this can become reversed in the case of some mesopelagic fish (Catul et. al., 2011). The relationships between fish larvae and siphonophores in the region is documented; therefore even if regions are identified as one scattering type it is more likely to represented a grouping of associated fauna (Sanvicente-Añorve et. al., 2007).

IDs 1 and 4 could represent a similar mixture of organisms of different sizes with the resonant frequency or Raleigh-geometric transition occurring at lower frequencies in ID1 implying larger sizes of the scaterers; but their locations are quite distinct and the structures and times at which they are observed differ significantly although their depth range is similar. When the euphausiid-like scattering type ID6, (Stanton et. al., 1994), is identified it always occurs in conjunction with these two ID4 and suggests that ID4 is a mixture of ID6 with another scattering type, potentially, siphonophores. ID1, although scattering a lot like ID1 across frequencies, occurs in very different areas and was selected for its characteristic 120 kHz to 200 kHz. This occurs in schools, predominantly near the seamount, in the surface layers and near the shelf break and may represent a dominant scattering type rather than a mixture of organisms that dominate different frequency ranges such as ID4. ID4 can be confidently attributed to Euphausiid sp. Along with ID6, since its patchy formation 100 to 150m depth, vertical migrations speeds and frequency thresholds all follow the observations of a number of publications[4]. Figure 29 shows the time-averaged echograms for the top 200m of water for 18 kHz on the left and 200 kHz on the right. The "patch" appearance at 1200hrs near the surface is also present at 120kHz but at reduced (S_A). The characteristically patchy region of the scattering at 120 kHz and 200 kHz rising in a step-wise fashion from 110m ahead of

[4] (Benoit-Bird & Whitlow, 2002); (Wiebe P. , et al., 1996); (Watkins & Brierley, 2002); (Benoit-Bird K.J., 2001)

each of the dominant DVM layers ascend at 0.17m/min in the shelf break region and 0.29m/min in the warm core. This is a speed consistent with the vertical migration of Euphausiid sp. and presents an expected increase for oligotrophic conditions (Pearre, 2003).

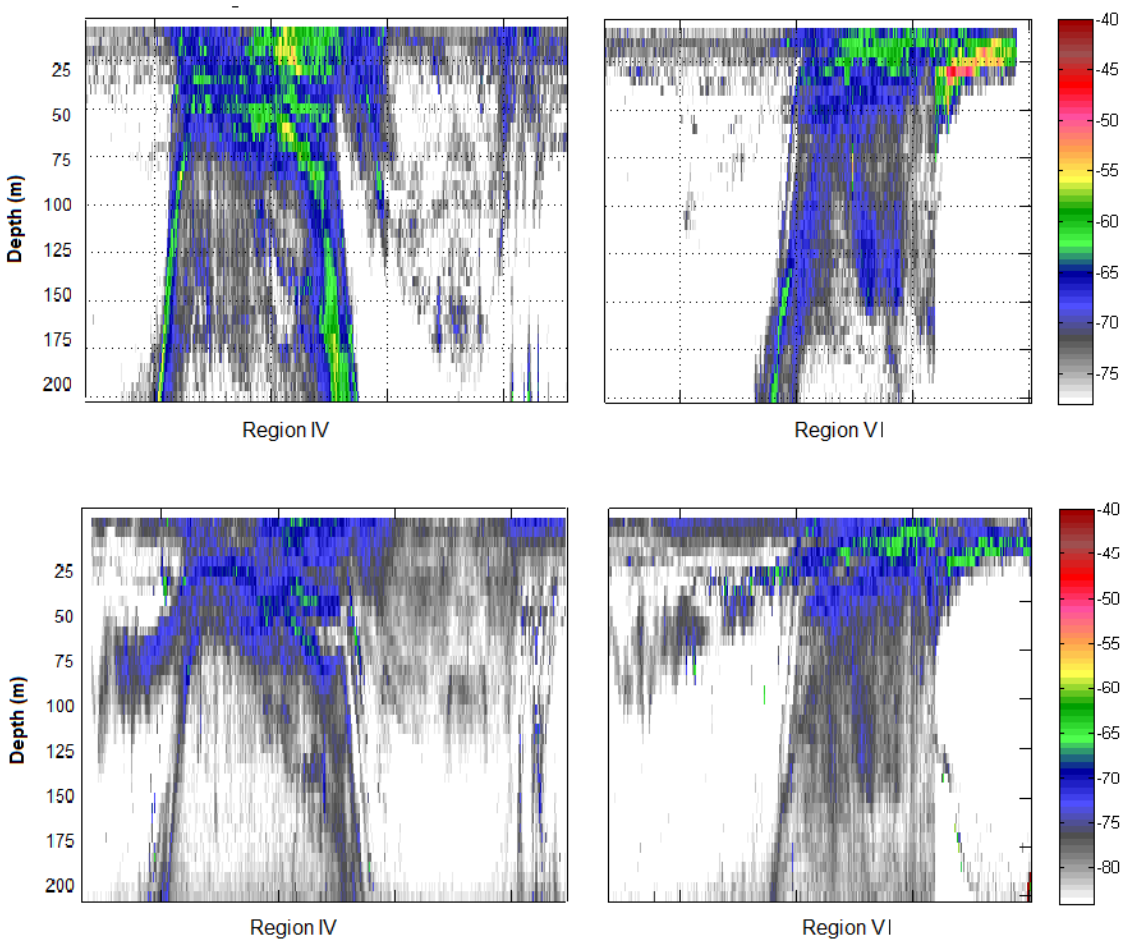

Figure 29: Echograms of the warm core ring (left, Region IV) and over a warm jet that extends over the NECS shelf (right, data not presented) at 18 kHz (top) and 38 kHz (bottom)

ID2 is singled out, but presents very different distributions. Within the top 200m of the water column it is exclusive to small patches in the surface waters and occurs exclusively in the top 180m of water after the DVM layer descent inside the warm core ring. But at depth this same trademark increase in reflected acoustic energy between 18 kHz and 38 kHz is associated with deep (450m to 700m) non migrating layers. It is unlikely that the scattering of ID2 making a diel migration to 200m would have

the same identity as a non-migrating deep layer. Furthermore, ID2 scatterers are identified as being quite distinct in Figure 24. It's frequency response makes it a prime candidate for the use of a bent cylinder model to be applied, and parameters from (Yasuma et. al., 2003) are used to obtain very similar frequency response (Figure 30). The identity of ID2 scatterers in the surface layers could be jelly fish as characterized by the significant drop between 38 kHz and 120 kHz, by reference to data collected in the Norwegian fjords (personal communication Thor Klevjer, KAUST/ University of Oslo), though no data is available at 18 kHz. It is also conceivable that this type of scattering relates to very small siphonophores and/or fish larvae to create a resonant frequency at 38 kHz, though scattering levels do suggest something without a swimbladder.

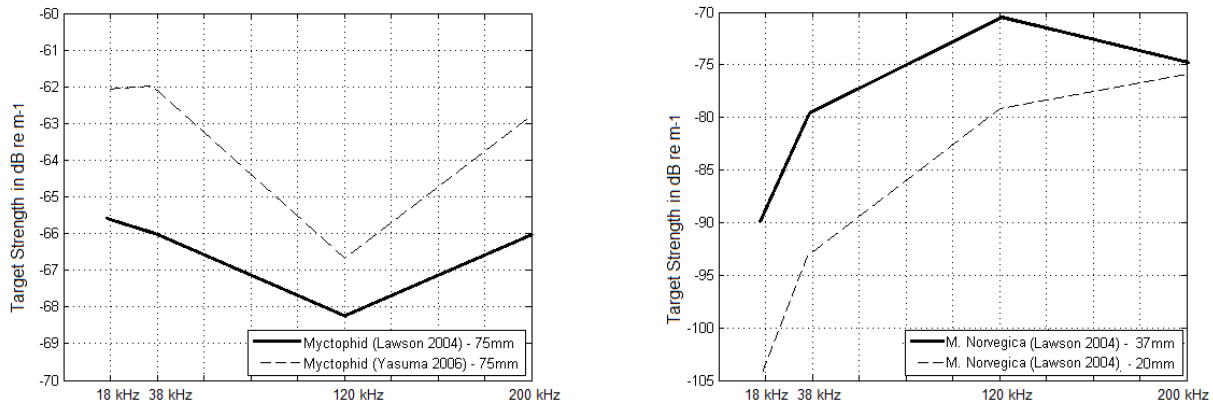

Figure 30: Examples of TS models built from the DWBA Bent cylinder physical model, illustrating the dependence of frequency response on dimensions and acoustic properties. Showing differences in acoustic properties (left) between Lawson (g=1.03, h=1.03) and Yasuma (g=1.035, h=1.055) and in Length (right).

The models in Figure 30 are both models, configured about the DWBA bent cylinder model. With the ID3 curves in mind from Figure 28, there is distinct similarity between the scattering observed in our data and the model of bent cylinder adjusted to the parameters set out in (Lawson et. al., 2004).

Myctophids form an important part of the deep scattering layer, and some, though not all, perform extensive dial vertical migration (DVM) between the epipelagic and mesopelagic regions (Catul et. al.,

2011). DVM is a widespread behaviour among pelagic species including zooplankton and mesopelagic fishes and this phenomenon presents considerable variation between species (Cisewski, Strass, & Kragefsky, 2010). In the Arabia Sea, Lanternfish are capable of DVM speeds reaching 3.3 m/min and migration distance around 400m and typically exhibit faster descents than ascents as in our case (Ashjian, Smith, Flagg, & Nasseer, 2002)&(Luo, Ortner, Forcucci, & Cummings, 2000). This agrees well with the results for the principal DVM layer in the data set and differs greatly from *Salpa aspera*, for example, which performs a DVM of at least 800m at 10 m/min (Wiebe, Maidn, Haury, Harbison, & Philbin, 1979), or Euphausiid migrations off the coast of California extending from depths of ~200m at 0.7m/min during descent and 0.3m/min during ascent (Pagès & Gili, 1991). This sets the stage for the use of ecological or statistical data to classify acoustic data moving towards a probabilistic classification technique (Anderson & Horne, 2007) , which makes use of ecological data such as aggregation densities, swimming speeds, migration tracks and timing in addition to TS model-based classification. Indeed, (Cisewski, Strass, & Kragefsky, 2010) is able to resolve acoustic scatterers into two categories of deep and shallow migrators, who travelled at 0.12-.18m/min and 0.04 to 0.12 m/min respectively, attributed to different zooplankton assemblages; where (Wiebe, Copley, & Boyd, 1992) find swimming speeds for copepods of 0.06 to 0.4 m/min. It is clear from such swimming speeds and frequency responses that the data does not show typical signals associated with salps or copepods as dominant scatterers within the data set.

Biomass estimates and Length Distributions

All biomass estimates are given in g/m^3 ; the swimbladderless fish model using (Yasuma et. al., 2006)' parameters adapted to the DWBA bent cylinder model will be adopted for the inversion process for estimations concerning ID3 and ID5. The fish with swimbladder model of a penetrable gas sphere and bent cylinder using the bladder diameter to length data from (Yasuma et. al., 2010) will

be used for estimates of ID2 biomass beyond 200m depth, and the *Meganyctiphanes norvegica* model from G.Lawson will be used for the ID4 scattering. All models are as described in the "Methodology Results" section, Figure 8.

Near the continental shelf, a full DVM is used for deriving estimates, rising from beneath 500m at 1900hrs. This DVM, like all other dominant vertical migrations patterns shows a synchronous ascent phase, with strongest scattering by ID5 at (0.281±0.01 g/m^3) during the ascent (ID3, 0.099±0.003 g/m^3); the scattering pattern becomes more diffuse along a constant depth line as the layer rises leaving a residual (ID5, 0.076±0.001 g/m^3) and (ID3, 0.038±0.001 g/m^3) below the ascending layer. Descent estimates are lower and more scattered in response time over the shelf break (ID5, 0.08±0.002 g/m^3) and (ID3, 0.071±0.003 g/m^3) or a third and three quarters of the ascending density for ID5 and ID3 respectively. The surface layer provided a density estimate of (ID5, 0.083±0.001 g/m^3) and (ID3, 0.036±0.002 g/m^3) before the arrival of the deep layer, at which point it soars to (ID5, 0.210±0.03 g/m^3) and (ID3, 0.170±0.03 g/m^3) or roughly 3 and 4 times the biomass density of the surface non-migrating layer for ID5 and ID3 respectively. The deep non migrating layer produces estimates of (ID2, 0.080±0.001 g/m^3) and (ID3, 0.029±0.001 g/m^3) near the shelf break or roughly a quarter and a sixth of the biomass density of the surface layer respectively (ID2 at surface, 0.280±0.001 g/m^3). In the slope waters these estimates drop to (ID2, 0.058±0.001 g/m^3) and (ID3, 0.022±0.001 g/m^3).

By comparison, the DVM observed in the warm core ring produces almost symmetrical density estimates for the ascending and descending layers of (ID5, 0.135±0.001 g/m^3) and (ID5,0.141±0.001 g/m^3) where estimates for ID3 give (ID3, 0.063±0.001 g/m^3) and (ID3,0.055±0.001 g/m^3). These are lower densities than the equivalent near-continental shelf-break DVM densities by a factor of 2.

Within the warm core ring, the surface backscatter forms a visibly thicker layer than it does near the shelf, suggesting oligotrophic waters from the assumption that primary productivity, in oligotrophic waters, extends to greater depths in sufficient quantities to support the migrating layers and certain

organisms would be encouraged to remain at depth due to predatorily pressures. The alternative, suggested by G.Lawson, that these layers are not feeding on phytoplankton would support the biological distinctness of the warm core ring as compared to the shelf break region. The surface phase of the DVM forms in bands with ID5 producing a layer at (0.27±0.03 g/m^3) biomass in between ID3 bands of (0.124±0.004 g/m^3). This region presents the highest densities seen at any point in the DVM layers, *cf.* Figure 16. This may suggest that scattering types are benefitting from the upwelling that is expected at the edge of the warm core ring and having to pack into much more dense patches to avoid predation. The residual scattering beneath the migrating layer, still in the top 100m produces similar estimates to those on the continental shelf of New England, at (ID5, 0.086±0.002 g/m^3), (ID3, 0.016±0.001 g/m^3).

Asymmmetry is expected in diurnal cycles as a starved mesopelagic layer ascends in unison with the light cue and feeds in the productive waters until satiated or threatened by the increasing light levels at dawn. This results in a less coherent descent in the diel cycle in productive waters (Pearre, 2003). In the case of oligotrophic waters a much more symmetrical distribution takes shape, both in its structure, densities and timing. The organisms within the warm core ring are taking the maximum amount of feeding time available to them and descending in synchrony again. Furthermore, it is unlikely that this phenomenon is due to the biomass within the warm core ring being composed of fewer species, since, as in the shelf break region, identical splitting of the ascending layer is observed in the top 50m of water into a quickly ascending layer, a continuation of the dominant DVM layer and a layer that remains some depth below the surface.

Considering the observations from the initial integrated volume backscatter results and the relative frequency responses of DVM layers, the densities obtained seem to confirm suspicions that the warm core ring as an abundant ecosystem, that forms greater density of layers in the clearer water and whose layers separate by vast regions of low backscatter. ID2 is nevertheless uniformly identified as the dominant scatterer remaining after descent of the surface layer, even in regions with quite low

backscatter. This may mean that scatterer ID2 is not just dominant but relatively-speaking the only scattering organism at this phase of DVM in the warm core ring.

In the top 200m no obvious trend between depth or phase of DVM were noticeable for the size distributions of our inversions. In the full water column where identification over greater depth is possible, but the applicability of the TS-model is less certain, the tendency was to fill in smaller size classes higher up in the water column for the ID2 model as well as for them to play a potentially bigger role in terms of biomass. The ID3 model shows almost no variation in the size classes filled. Whether this is due to the match of the inversion to frequency response, to the code itself is unclear at this point.

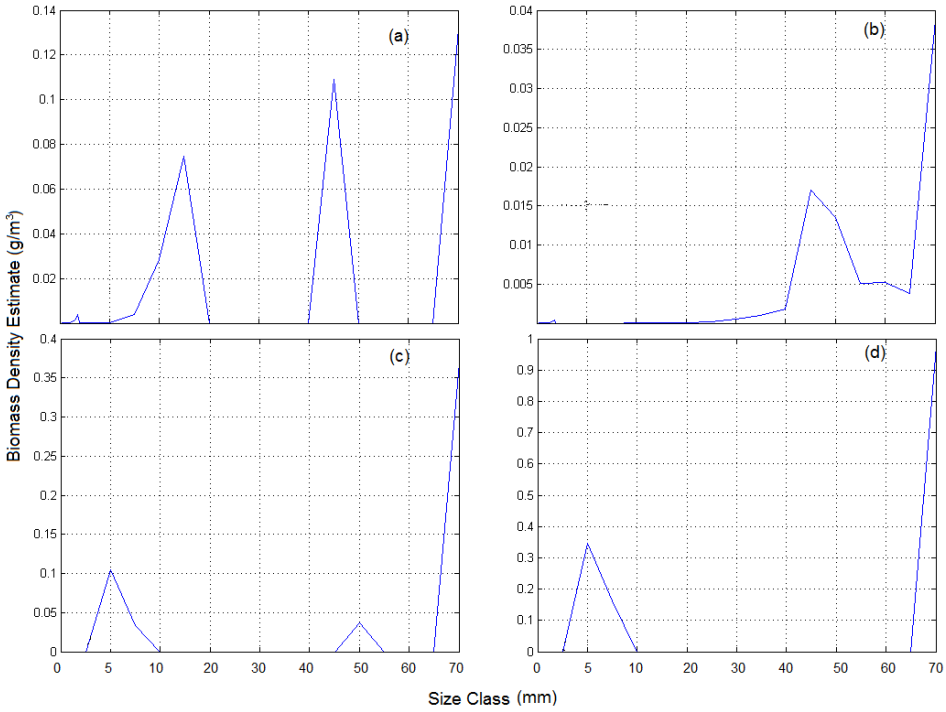

Figure 31: Length Distributions over the size classes (x-axis) between 0.5mm and 70mm for ID2 at positions (a) Region I at 50m depth, (b) Region I at 500m depth, (c) Region I at 200m depth and (d) Region II at 200m depth.

Roughly two thirds of the scattering organisms inhabiting the 400 to 700m depth range during the day ascend to the surface on the continental shelf. Virtually no change in density is observed across the depth range of the remaining non-migrating layer for ID3 and ID2. The descending layer in the warm core ring seems to roughly split in half of its density at the beginning of the DVM descent: i.e

from (0.055±0.001 g/m^3) to (0.020±0.001 g/m^3) in the shallower migrating layer down to 500m and to (0.021±0.001 g/m^3) in the deeper migrating layer down to 650m.

Within the non-migrating layers at daytime, there is a reduction in maximum density of the scattering types that is strongly stratified by depth as well as strong similarity in density values along depth lines. This seems to be true for both scattering type ID3 and ID2, though it is not testable for ID5. The phenomenon is not observable during the night due to the inevitable intervention of the movements and density changes cause by the dial cycle with the stratification observed at day. This suggests that within scattering types there is an optimum density balanced between environmental conditions such as light levels and predation.

Previous studies find similar distinct compositions between semi-subtropical species dominating the warm core ring, as opposed to temperate-species dominating the shelf break waters and low abundance in slope waters outside the warm core ring (Cradock, 1989). Fish Biomass only represented a quarter of zooplankton biomass (Boyd, 1968), which echoes our higher biomass densities for ID2 over ID3 in shallow waters. They also find that fish biomass is almost exclusively restricted to below 250m at day, only approaching near surface at night (Boyd, 1986). From our results, ID3 should contain a gas inclusion, unlikely to be a siphonophore due to the resonant frequency being smaller than 18 kHz. This unfortunately leaves ID2, the next dominant scatterer, as well as other IDs not detectable to below 200m with an enormous variety of options: the higher scattering at 38 kHz than 18 kHz favouring organisms with very small or negligible swimbladders. In Cradock and Boyd's studies, strong migrators were dominated by myctophids while deep non-migrating layers were dominated by Gonostromidae (Cyclothone sp.), exhibiting a maximum catch between 700 and 750m depth (Cradock, 1989). More importantly, the catch rate is cited as one specimen per 10^4 m^3, which is significantly lower than our estimates.

WORKS CITED

Anderson, C., & Horne, J. (2007). Classifying multifrequency fisheries acoustic data using a robust probabilistic classification technique. *Acoustical Society of America* .

Anderson, C., Brierley, A., & and Armstrong, F. (2005). Spatio-temporal variability in the distribution of epi-and meso-pelagic acoustic backscatter in the Irminger Sea, North Atlantic, with implications for predation on Calanus finmarchicus. *Marine Biology* , 146(6): 1177-1188.

Ashjian, C., Smith, S., Flagg, C., & Nasseer, I. (2002). Distribution, annual cycle, and vertical migration of acoustically derived biomass in the Arabian Sea during 1994-1995. *Deep Sea Research II* .

Backus, R. C., Shores, D., Teal, J., & Wing, A. (31 May 1968). Ceratoscopelus madrensis: Peculiar Sound-Scattering Layer Identified with This Mycotphid Fish. 992-993.

Badcock, J., & Merrett, N. (1975). Midwater fishes in the eastern North Atlantic - I. Vertical distribution and associated biology in 30°N,23°W, with developmental notes on certain myctophids. *Progress in Oceanography* , Vol. 7, pp. 3-58.

Badcock, J., & Merrett, N. (1976). Midwater fishes in the eastern North Atlantic - I. Vertical distribution and associated biology in 30°N,23°W, with developmental notes on certain myctophids. *Progress in Oceanography* , Vol. 7, pp. 3-58.

Barrange, M. (1994). Acoustic identification, classification and structure of biological patchiness on the edge of the Agulhas bank and its relation to frontal features. *South African Journal of Marine Science* , Vol.14: 337-347.

Bemaish, R., Leask, K., Ivanov, O., Balanov, A., Orlov, A., & Sinclair, B. (1999). The ecology, distribution and abundance of midwater fishes of the Subarctic Pacific gyres. *Progress in Oceanography* , Issue 43, pp.399-442.

Benoit-Bird, K. a. (2001). Target Strength measurments of Hawaiian mesopelagic boundary community animals. *Journal of the Acoustic Society of America* .

Benoit-Bird, K. (2009). The effects of scattering-layer composition, animal size, and numerical density on the frequency resonse of volume backscatter. *ICES Journal of Marine Science* .

Benoit-Bird, K., & Au, W. (2006). Extreme diel horizontal migrations by a tropical nearshore resident micronekton community. *Marine Ecology Progress Series* , Vol. 319, 1-14.

Benoit-Bird, K., & Whitlow, W. (2002). Energy: Converting from acoustic to biological resource units. *Journal of the Acoustic Society of America* .

Bolz, G. L. (1978). Retention of Ichthyoplankton in the Georges Bank Region During the Atumun-Winter Seasons, 1971-1977. *Journal of the Northwest Atlantic Fisheries Sciences* , Vol. 5 33-45.

Boyd, S., Wiebe, P., Backus, R., & Craddock, J. a.-A. (1986). Biomass of the micronecktonin the Gulf Stream ring 82-B and environs changes with time. *Deep Sea Research I* , Vol 33 N° 11/12 pp. 1885-1905.

Burgos, J., & Horne, J. (2008). Characterization and classification of acoustically detected fish spatial distributions. *ICES Journal of Marine Science* , 1235-1247.

Catul, V., Gauns, M., & Karuppasamy, P. (2011). A review on mesopelagic fishes belonging to family Myctophidae. *Rev Fish Biol Fisheries* , 21:339-354.

CCAMLR. (1993). *Fish Resources: Fishery Status and Trends*. Consulté le September 21, 2011, sur Publications Series 1992: http://www.ccamlr.org/pu/e/e_pubs/sr/92/i3.pdf

Chapman, D.C and Beardsley, R.C. (1989). On the origin of the shelf water in the middle Atlantic Bight, J. Phys. Oceanogr. 19: 384-391.

Chu, D., Foote, K.G, and Stanton, T.K (1993). Further analysis of target strength measurements of Antarctic Krill at 38 and 120 kHz; Comparison with deformed cylinder model and inference of orientation distribution. *J. Acoust. Soc. Am.* 93, 2985-2988.

Cisewski, B., Strass, V. M., & Kragefsky, S. (2010). Seasonal variation of diel vertical migration of zooplankton from ADCP backscatter time series data in the Lazarev Sea, Antarctica. *Deep Sea Research I* , pp78-94.

Coetzee, J. (2000). Use of shoal analysis and patch estimation system (SHAPES) to characterize sardine schools . *Aquatic Living Resources* , Vol.13, pp. 1-10.

Cradock, J.E, Backus, R.H, Daher, M.A. (1989). Vertical distribution and species composition of midwater fishes in warm-core Gulf Stream meander/ring 82-H. Deep Sea Research, Vol.39.

Davidson, P. (2011). The specific gracity of mesopelagic fish form the northeastern Pacific Ocean and its implications for acoustic backscatter. *ICES Journal of Marine Science* .

De Robertis, A., & Higginbottom, I. (2007). Apost-processing technique to estimate the signal-to-noise ratio and remove echosounder background noise. *ICES Journal of Marine Science* , 1282:1291.

De Robertis, A., McKelvey, D., & Ressler, P. (2010). Developent and application of an empirical multifrequency method for backscatter classification. *Canadian Journal of Fisheries and Aquatic Sciences* , Vol.67: pp. 1459-1474.

De Robertis, A., McKelvey, D., & Ressles, P. (2010). Development and application of an empirical multifrequency method for backscatter classification. *Canadian Journal Fisheries and Aquatic Sciences* .

Echoview. (2009, October 21). *Hydroacoustic User Forum*. Consulté le September 21, 2011, sur http://hydroacoustics.net/viewtopic.php?f=2&t=549

Endo, Y., & Wiebe, P. (2004). Euphausiid distirbution, abundance, and succession in North Atlantic warm-core ring 82B. *Journal of Plankton Research* , Vol.27, N°2, pp. 175-188.

FAO. (2011). *FAO Coprorate Document Repository*. Consulté le 11 16, 2011, sur FAO: http://www.fao.org/docrep/X5818E/x5818e06.htm#TopOfPage

FAO. (1997). *Lanternfishes: a potential fishery in the northern Arabian Sea.* Rome: FAO fisheries, Available: http://www.fao.org/docrep/003/w4248e/w4248e34.htm. Last visit: September 2011.

Gauthier, S., & Horne, K. (2004). Acoustic characteristics of forage fish species in the Gulf of Alaska and Bering Sea based on Kirchoff-approximation models. *Canadian Journal of Fisheries and Aquatic Sciences* , Vol.61: 1839-1850.

Gjosaeter, J., & Kawaguchi, K. (1980). A review of the World's resources of mesopelagic fish. *FAO Fisheries Tech. Pap* .

Godo, O., Patel, R., & Pedersen, G. (2009). Diel migration and swimbladder resonance of small fish: some implications for analyses of multifrequency echo data. *ICES Journal of Marien Science* .

Ha, V. V. (2008). *Seperating Blue whiting from myctophid targets using multi-frequency methods* . Bergen: Unviersity of Bergen.

Hazen, L., Nowacek, D., St.Laurent, L., Halpin, P., & Moretti, D. (2011). The relationship among oceanography, prey fields and beaked whale foraging habitat in the tongue of the ocean. *Plos One* .

Hewitt, R., & Demer, D. (1993). Dispersion and abundance of antarctic krill in the vicinity of Elephant Island in the 1992 austral summer. *Marine Ecology Progress Series* , Vol 99, pp 29-39.

Hulley, P. (2011). *Iziko Museums*. Consulté le Novemebr 12, 2011, sur Latnern fish research: http://www.iziko.org.za/static/page/marine-biology

Isaaks, E., & Srivastava, R. (1989). *unknown.* unknown: unknown.

Jech, J., & Micheals, W. (2006). A multifrequency method to classify and evaluate fisheries acoustics data. *Canadian Journal of Fisheries and Aquatic Sciences* .

Kalikhman, I., & Yudanov, K. (2006). *Avoustic fish reconnaissance.* London - New York: CRC Press, Taylor and Francis Group.

Kane, J. (2011). Multiyear variability of phytoplankton abundance in the Gulf of Maine. *ICES Journal of Marine Science* , Vol.68 Iss.9 pp. 1833-1841.

Karuppasamy, P., George, S., & Menon, N. (2008). Length-weight relationship of the Benthesoma pterotum (myctophid) in the deep scattering layer (DSL) of the easter Arabian Sea. *Indian Journal of Fisheries* , 301-303.

Kelly, N., Shea, E., Metexas, A., Haedrich, R., & Auster, P. (2010). Biodiversity of the Gulf of Maine (NW Atlantic): Relationships among Sub-Regions and to Shelf Systems. *PlosONE* , Vol5, Issue11, ov2011.

Kenney, R. a. (1985). Cetacean biomass densities near submarine cnayons cmpared to adgacent shelf/slope areas. *Continental Shelf Research* , Vol 7, N°2, pp107-114.

Kinzer, J., Bottger-Schnack, R., & Schulz, K. (1993). Aspects of horizontal distribution and diet of myctophid fish in the Arbian Sea with reference to the deep water oxygen deficiency. *Deep Sea Research II* , Vol.40, N°3, pp.783-800.

Korneliussen, R., & Ona, E. (2002). An operational system for processing and visualizing multi-frequency acoustic data. *ICES Journal of Marine Science* , Vol.59; 292-313.

Krefft, G. (1976). Distribution of mesopelagic fishes in the equatorial and western North Atlantic Ocean -- International Overflow '73 Expedition of ICES. *Revue des Travaux de l'Institut des Peches Maritimes* .

Lavery, A.C , Wiebe, P. , Stanton, T.K , Lawson, G.L , Benfield, M.C , Copley, N. (2007). Determining dominant scatterers of sound in mixed zooplankton populations. Journal of the Acoustical Society of America.

Lawson, C., & Hanson, R. (1973). Solving Least Squares Porblems. *Pretince-Hall* .

Lawson, G., Wiebe, P., Ashjian, C., & Stanton, T. (2007). Euphausiid distribution along the Western Antarctic Peninsula, Parts A&B. *Deep Sea Research II* .

Lawson, G., Wiebe, P., Ashjian, C., Gallager, S., Davis, C., & Warren, J. (2004). Acosutically-inferred zooplankton distribution in relation to hydrography west of the Antarctic Peninsula. *Deep Sea Research II* , 2041-2072.

Lawson, Wiebe, P., Ashjian, C., Dezhang, C., & Stanton, T. (2006). Improved parametrization of Antarctic krill target strength models. *Journal of the Acoustical Society of America* , pp. 232-242.

Luo, J., Ortner, P., Forcucci, D., & Cummings, S. (2000). Diel vertical migration of zooplankton and mesopelagic fish in the Arabian Sea. *Deep Sea Research II* .

Mann, K., & Lazier, J. (1996). *Dynamics of marine ecosystems: biological-physical interactions in the oceans.* Oxford: Wiley-Blackwell, pp.271-275.

Mayo, R., & Serchuk, F. (1987). Aggergate Fish Biomass and Yield on Geroges Bank, 1960-87. *Journal of Northwest Atlantic Fisheries Science* , Vol 14: 59-78.

McGinnis, R. (1982). Biogeography of the lantern fishes (Myctophidae) south of 30°S. *Washington, D.C. : American Geophysical Union, Antarctic Research Series* , 35:110.

McLennan, & Simmons. (1992). Fisheries Acoustics.

Morel, A. (1988). Optical Modeling of the Upper Ocean in Relation to Its Biogenous Matter Content (Case I Waters). *Journal of Geophysical Research* , Vol.93, pp.749-768.

Moteki, M., Koubbi, P., Pruvost, P., Tavernier, E., & Hulley, P. (2011). Spatial distribution of pelagic fish off Adélie and George V Land, East Antarctica in the austral summer 2008. *Polar Science* , Vol 5. Issue 2.

NEFMC. (2011). *The New England Fishery Management Council Mission Statement.* Newburyport: The New England Fishery Management Council, Available at. http://www.fisherycouncils.org/USFMCsections/USRFMCnefmc.pdf, last Accessed: September 2011.

NOAA. (2011, September 21). *Coastwatch West Coast Regional Node*. Consulté le September 21, 2011, sur NOAA- Bloomwatch 360: http://coastwatch.pfel.noaa.gov/coastwatch/CWBrowserWW360.jsp

NOAA. (2009). *NOAA Fisheries Service, Marine Mammal Survey, 6-16th August, 2009, HB 09-03.* Woods Hole: Northeast Fisheries Science Center.

NOAA. (2011, September 21). *NOAA Ship Henry Bigelow Electronics Suite*. Consulté le September 21, 2011, sur NOAA Marine Operations' Henry Bigelow Website: http://www.moc.noaa.gov/hb/specs/navigation.htm

O'Driscoll, R., Gauthier, S., & Devine, J. (2009). Acoustic estimates of mesopelagic fish: as clear as day and night? *ICES Journal of Marine Science* .

Pakhamov, E., Perissinotto, R., & McQuaid, C. (1996). Prey composition and daily rations of myctophid fishes in teh Southern Ocean. *Marine Ecology Progress Series* , Vol 134:1-14.

Pearre Jr., S. (2003). Eat and run? The hunger/satiation hypothesis in vertical migration: history, evidence and consequences. *Cambridge Philosophical Society* , pp. 1 - 79.

Reeder, B., Jech, M., & Stanton, T. (2004). Broadband acoustic backscatter and high resolution morphology of fish: Measurement and modeling. *Journal of the Acoustic Society of America* .

Robinson, A.R and Brink, K.H. (2004). The Sea: The Global Coastal Ocean: Interdisciplinary Regional Studies and Syntheses. Chapter 5. Harvard University Press.

Ross, R., Quattrini, A., Roa-Varon, A., & McClain, J. (2010). Species composition and distributions of mesopelagic fishes over the slope of the north-central Gulf of Mexico. *Deep Sea Research II* .

Sanvicente-Añorve, L., Alatorre, A., Flores-Coto, C., & Alba, C. (2007). Relationships between fish larvae and siphonophores in the water column: effect of wind-induced turbulence and thermocline depth. *ICES Journal fo Marine Science* , 878-888.

Sawada, K., Uchikawa, K., Matsura, T., Sugisaki, H., Amakasu, K., & Abe, K. (2011). In situ and ex situ target strength measurement of mesopelagic lanternfish. *Journal of Marine Science and Technology* , 302-311.

Simard, Y., & Lavoie, D. (1999). The rich krill aggregation of the Saguenay - St. Lawrence Marine Park; hydroacoustic and geostatistical biomass estimates, structure, variability and significance for whales. *Canadian Journal of Fisheries and Aquatic Sciences* , Vol. 56 pp. 1182-1197.

Stanton, T.K, Wiebe, P.H, Chu, D., Benfield, M.C, Scanlon, L., Martin, L., Eastwood, R.L. (1994). On acoustic estimates of zooplankton biomass. *ICES J. Of Mar. Sci.* 51: 595-512.

Stanton, T.K, Chu, D., & Wiebe, P. (1996). Acosutic scattering characteristics of several zooplankton groups. *ICES Journal of Marine Science* , 289-285.

Stern, H., & Serchuk, F. (1992). *Scientific Council meeting for the Northwest Atlantic Fisheries Organization.* Woods Hole, MA: NOAA/NMFS.

Sullivan-Silva, K. (1st November1989). *Underwater Acoustic Scattering form Spherical Particulates and Bubbles, NUSC Technical Report, .* Newport, Rhode Island: Weapon Systems Technology and Assessment Department.

Swartzman, G., Brodeur, R., Napp, J., Walsh, D., Hewitt, R., Demer, D., et al. (1999). Relating spatial distributions of acoustically determined patches of fish and plankton: data viewing, image analysis and spatial proximity. *Canadian Journal of Fisheries and Aquatic Sciences* , Vol 56 pp. 188-198.

Turley, S. (unknown). *Acosutic Scattering form a gas-filled sphere*. Consulté le 11 07, 2011, sur http://volta.byu.edu/winzip/scalar_sphere.pdf

Watkins, J., & Brierley, A. (2002). Verification of the acoustic techniques used to dientify Antarctic krill. *ICES Journal of Marine Science* , 1326-1336.

Wiebe, P., Ashjian, C., Gallager, S., Davis, G., Lawson, G., & Copeley, N. (2004). Using a high powered strobe light to increase the catch of Antarctic krill. *Marine Biology* , 493 - 502.

Wiebe, P., (1988) Functional Regression equations for zooplankton displacement volume, wet weight, dry weight, and carbon: a correction. *Fish. Bull.,* 73: 777-786.

Wiebe, P., Copley, N., & Boyd, S. (1992). Coarse scale horizontal patchiness and vertical migration of zooplankton in Gulf Stream warm-core ring 82-H. . *Deep Sea Research I* .

Wiebe, P., Maidn, L., Haury, L., Harbison, G., & Philbin, L. (1979). Diel Vertical Migration by Salp aspera and its Potential for Large-Scale Particulate Organic Matter transport to the Deep Sea. *Marine Biology* , Vol 53, pp249-255.

Wiebe, P., Mountain, D., Stantion, T., Greene, C., Lough, G., Kaarvedt, S., et al. (1996). Acoustical Study of the spatial distribution of plankton on Georges Bank and the relationship between volume backscattering strength and the taxonomic composition of the plankton. *Deep Sea Research II. Vol 43, N° 7-8* .

Wiebe, P., Mountain, D., Stanton, T., Lough, G., Kaartvedt, S., Dawson, J., et al. (1996). Acoustical study of the spatial distribution of plankton on Georges Bank and the relationship between volume bckscattering strength and taxonomic composition of the plankton. *Deep Sea Research II* , Vol.43, N° 7-8, pp1971-2001.

Yasuma, H., Sawada, K., Ohshima, T., Miyashita, K., & Aoki, I. (2003). Target strength of mesopelagic lanternfishes (family Myctophidae) absed on swimbladder morphology. *ICES Journal of Marine Science* , Vol.60: pp. 584-591.

Yasuma, H., Sawada, K., Takao, Y., Miyashita, K., & Aoki, I. (2010). Swimbladder condition and target strength of myctophid fish in the temperate wone of the Northwest Pacific. *ICES Journal of Marien Science* , Vol.67: 000-000.

Yasuma, H., Takao, Y., Sawada, K., Miyashita, K., & Aoki, I. (2006). Target strength of Stenobrachius leucobrachius in the Bering Sea. *ICES Journal of Marine Science*.